

# Ethical Fairness without Demographics in Human-Centered AI

SHAILY ROY, HARSHIT SHARMA, and ASIF SALEKIN, Arizona State University, USA

Computational models are increasingly embedded in human-centered domains—healthcare, education, workplace analytics, and digital well-being—where their predictions directly influence individual outcomes and collective welfare. In such contexts, achieving high accuracy alone is insufficient; models must also act ethically and equitably across diverse populations. However, fair AI approaches that rely on demographic attributes are often impractical, as such information is often unavailable, privacy-sensitive, or restricted by regulatory frameworks. Moreover, conventional parity-based fairness approaches, while aiming for equity, can inadvertently violate core ethical principles—by trading off subgroup performance or stability. To address this challenge, we present **FLARE**—Fisher-guided LAtent-subgroup learning with do-no-harm REgularization, the first demographic-agnostic framework that aligns algorithmic fairness with ethical principles through the geometry of optimization. **FLARE** leverages Fisher Information to regularize curvature, uncovering latent disparities in model behavior without access to demographic or sensitive attributes. By integrating representation, loss, and curvature signals, it identifies hidden performance strata and adaptively refines them through collaborative but do-no-harm optimization—enhancing each subgroup’s performance while preserving global stability and ethical balance. We also introduce BHE (Beneficence–Harm Avoidance–Equity), a novel metric suite that operationalizes ethical fairness evaluation beyond statistical parity. Extensive evaluations across diverse physiological (EDA), behavioral (IHS), and clinical (OhioT1DM) datasets show that **FLARE** consistently enhances ethical fairness compared to state-of-the-art baselines. Comprehensive ablation and loss-landscape analyses validate its design principles, and runtime evaluations confirm its practicality for resource-constrained edge deployment.

## ACM Reference Format:

Shaily Roy, Harshit Sharma, and Asif Salekin. 2024. Ethical Fairness without Demographics in Human-Centered AI. *ACM J. Auton. Transport. Syst.* 0, 0, Article 0 (2024), 32 pages. <https://doi.org/XXXXXXX.XXXXXXX>

## 1 Introduction

Artificial intelligence (AI) is rapidly becoming a cornerstone of modern healthcare, integrating data-driven intelligence across human-sensing domains to enhance diagnosis, risk prediction, and continuous monitoring—transforming raw multimodal data from health records, medical images, and wearables into actionable, personalized insights [53, 71, 87, 88, 100, 103]. Yet these gains come with a persistent risk: performance is not uniform. Hidden heterogeneity in physiology, behavior, context, and device usage often yields uneven performance across subgroups, many of which are latent [2, 24, 90]. Consequently, models that perform well on average can still systematically underserve specific groups, embedding inequities into decision pipelines and emphasizing the need for subgroup-aware fairness-driven learning approaches [5].

Recent U.S. policy developments—such as updates to the Health and Human Services (HHS) nondiscrimination rule and new federal AI governance frameworks—emphasize equitable and privacy-oriented ML in healthcare [4, 85]. This vision is echoed in the 2025 Executive Order [34], which calls for bias-resistant, innovation-driven AI that advances fairness *through principled optimization rather than demographic categorization*, fostering equity without reinforcing engineered social constructs.

---

Authors’ Contact Information: Shaily Roy, [shailyro@asu.edu](mailto:shailyro@asu.edu); Harshit Sharma, [hsharm62@asu.edu](mailto:hsharm62@asu.edu); Asif Salekin, [asalekin@asu.edu](mailto:asalekin@asu.edu), Arizona State University, Tempe, Arizona, USA.

---

Permission to make digital or hard copies of all or part of this work for personal or classroom use is granted without fee provided that copies are not made or distributed for profit or commercial advantage and that copies bear this notice and the full citation on the first page. Copyrights for components of this work owned by others than the author(s) must be honored. Abstracting with credit is permitted. To copy otherwise, or republish, to post on servers or to redistribute to lists, requires prior specific permission and/or a fee. Request permissions from [permissions@acm.org](mailto:permissions@acm.org).

© 2024 Copyright held by the owner/author(s). Publication rights licensed to ACM.

ACM 2833-0528/2024/0-ART0

<https://doi.org/XXXXXXX.XXXXXXX>

In human-centered AI—especially in healthcare—fairness is deeply intertwined with ethics. Ethical AI must not only ensure equitable performance but also uphold the principles of *beneficence* (promoting overall benefit), *non-maleficence* (avoiding harm), *justice* (ensuring equitable treatment), and *autonomy* (maintaining stability) [8, 23, 36]. Yet, conventional fairness-driven optimization often overlooks these broader ethical dimensions. Methods that focus narrowly on equalizing performance can inadvertently mask subgroup failures, reduce collective benefit, and erode trust in human-centered applications [72]. This underscores a critical need: fairness and ethical principles must be systematically integrated into AI model design and optimization to ensure reliable, trustworthy, and impactful use in sensitive human-centered domains such as healthcare.

Guided by these imperatives, this paper’s *goal* is to develop human-centered AI models that (i) maximize both overall and subgroup-wise accuracy, (ii) reduce disparities, thus improving stability across both subgroups and individuals—without relying on sensitive demographic information or prior knowledge of those subgroups, and (iii) enforce non-degradation so that no subgroup performs worse than a baseline.

A central challenge in attaining this *goal*, as discussed above, is that the information on demographics or sensitive attributes may be unavailable, or undesirable due to privacy, regulatory, or ethical concerns [9, 21, 70, 80]. Fairness, therefore, should be pursued through model behavior rather than demographic supervision. We approach this through the lens of optimization geometry: the curvature of the loss landscape is tightly linked to robustness, i.e., stability and subgroup disparities. Loss-landscape sharp regions—captured by the high Hessian—are associated with parameters that are highly sensitive to perturbations; subgroups concentrated near such regions tend to lie closer to decision boundaries and experience less stable performance than others [17, 39, 84]. Because computing full Hessians is prohibitive at scale, following the literature [51, 62, 83, 96], we adopt Fisher Information as a tractable surrogate that preserves key curvature properties.

Thus, *to attain the above-discussed goal*, this paper introduces **FLARE**—Fisher-guided LAtent-subgroup learning with do-no-harm REgularization. This demographic agnostic framework aligns fairness with ethical principles by explicitly shaping and leveraging the loss landscape: Through Fisher-informed curvature regularization, **FLARE** learns smoother loss landscapes and more stable decision boundaries, reducing sensitivity to perturbations and enhancing generalizability—thus reinforcing the ethical principle of *autonomy* (*goal-ii*) through stability and reliability. Next, it discovers latent subgroups through joint analysis of embedding similarity, prediction loss, and curvature response—exposing where model behavior diverges across populations. In doing so, **FLARE** reveals the disparities in model behavior across latent subgroups, even in the absence of demographic labels—thereby advancing the ethical principle of *justice* (*goal-ii*). Finally, **FLARE** refines model behavior by training latent subgroup-specific extensions through a conditional aggregation, enhancing inter- and intra- subgroup performance, fairness, and stability, while ensuring that no subgroup deteriorates as fairness improves. This design operationalizes *beneficence* (*goal-i*) and *justice* (*goal-ii*) by improving collective performance and equity, and *non-maleficence* (*goal-iii*) by safeguarding against subgroup harm. Together, these mechanisms yield ethically grounded AI systems that balance efficacy, fairness, and stability across diverse human populations.

This work’s primary contributions, embodied in **FLARE**, are:

- **Ethical fairness without demographics:** It introduces **FLARE**, the first human-centered framework that enforces fairness and ethical consistency without relying on demographic attributes. By integrating *model representation-behavior fusion*—combining embeddings, cross-entropy loss, and Fisher Information—**FLARE** uncovers latent performance strata, identifies underserved subgroups, and promotes ethically constrained fairness across them, all while remaining agnostic to demographic or other sensitive attributes.
- **Do-no-harm adaptation:** It presents a novel do-no-harm training mechanism that enhances the performance of underserved or underperforming subgroups without degrading others. This design operationalizes the ethical principles of *beneficence* (improving outcomes) and *non-maleficence* (avoiding harm), while maintaining global equity and model stability.

- **Ethics-grounded evaluation metrics:** To address the lack of principled evaluation tools, it introduces the *BHE* (Benefit, Harm-avoidance, Equity), a new metric suite, which directly ties empirical model behavior to core AI ethics principles—quantifying how well a model balances collective improvement, subgroup protection, and equity in performance variance.
- **Comprehensive Empirical Validation and Justification.** Through extensive evaluation across physiological (EDA), behavioral (IHS), and clinical (OhioT1DM) datasets, **FLARE** demonstrates that fairness, constrained by ethics, can be seamlessly integrated into real-world human-centered AI systems. These experiments confirm that **FLARE** achieves its above-mentioned goals: (*goal-i*) improved overall and subgroup-wise accuracy (Section 6.2.1), (*goal-ii*) reduced disparities, thus enhanced stability across subgroups (Section 6.2.2) and individuals (Section 6.2.3), while (*goal-iii*) ensuring non-degradation of any subgroup, both internal to **FLARE** steps (Section 6.2.4), and compared to established baselines (Section 6.2.2). Ablation and loss-landscape analyses validate its principled design (Section 6.3), while runtime evaluations on diverse edge platforms (Section 7) confirm its scalability and readiness for trustworthy, equitable deployment.

## 2 Related Work

This section reviews related work on algorithmic fairness and ethical AI. We begin with methods that rely on demographic information, then discuss fairness approaches that operate without sensitive attributes, subgroup-oriented fairness techniques, and recent efforts to align fairness with ethical and human-centered principles in healthcare.

### 2.1 Fairness through Demographic Information

Early algorithmic fairness methods relied on demographic attributes to constrain predictions [9, 25, 70]. Preprocessing methods, such as reweighting or relabeling, reduced training data bias but did not ensure fair representations or predictions under complex decision boundaries [42]. In-processing techniques addressed this by incorporating fairness directly into the learning objective by modifying loss functions or adding regularizers, enforcing parity in error rates or decision boundaries [98, 99]. These methods offered finer control but often traded off with overall accuracy. Post-processing strategies adjusted outputs after training, for example by shifting thresholds or randomizing predictions, to satisfy criteria like demographic parity or equalized odds [28, 64, 89]. While simple and flexible, they left underlying representations unchanged and were unstable in deployment [22, 28]. Overall, demographic-based methods established the foundation of fairness research but remain limited by their dependence on sensitive attributes—often unavailable or undesirable in domains such as human sensing [21, 70].

### 2.2 Fairness without Demographic (FWD)

The growing need for fairness without relying on sensitive demographic attributes has driven new approaches to mitigate bias [14, 46, 49]. Adversarial reweighting dynamically adjusts instance weights during training to emphasize underperforming or misclassified samples, thereby mitigating disparities across hidden subgroups [49]. However, such reweighting can destabilize optimization and often reduces overall accuracy, since amplifying difficult instances may distort the training objective. Another direction is knowledge distillation (KD), where a complex teacher model transfers knowledge to a simpler student model. Adapted to fairness, this approach allows the student to inherit subgroup performance improvements from the teacher without requiring access to demographic attributes [14]. Yet KD-based methods remain highly dependent on the quality of the teacher model; if the teacher encodes biased representations, those biases may be propagated or even amplified in the student. Furthermore, distillation often struggles to generalize to underrepresented subgroups, limiting its ability to ensure equitable outcomes. Ni et al. propose *Reckoner* [68], a confidence-based hierarchical framework for fairness without sensitive attributes. *Reckoner* partitions data into high- and low-confidence subsets and trains

dual models that exchange pseudo-label information to reduce the influence of biased features. Learnable noise is injected to mitigate label bias, and the framework achieves improved fairness–accuracy trade-offs across tabular datasets. Despite these gains, *Reckoner*’s reliance on confidence-based partitioning can make its performance sensitive to threshold selection and model initialization. Luo et al. introduce Graph of Gradients (GoG) [59], showing that last-layer gradients correlate more strongly with unobserved sensitive subpopulations than raw features. GoG formulates a Rawlsian max–min objective through an adversarial reweighting game: for each minibatch, it computes per-example losses and last-layer gradients, constructs a  $k$ -NN graph in gradient space, and passes these node features through a one-layer GCN to produce instance weights. This design enables the adversary to emphasize locally coherent “gradient neighborhoods” instead of isolated hard samples, stabilizing training compared to instance-wise reweighting. However, GoG’s success depends heavily on the stability of  $k$ -NN graph construction and the expressivity of its shallow GCN, which can suffer from over-smoothing and sensitivity to noise [35, 43]. While prior approaches aim to make model behavior uniformly fair, such unguided optimization often complicates training and risks degrading performance. Our perspective instead is that fairness can be achieved more effectively by identifying and addressing *latent disparities*—hidden differences in how models treat similar and dissimilar instances. This targeted strategy simplifies optimization, provides structure to fairness adjustments, and enables more stable learning.

Given their relevance and demonstrated impact, we adopt adversarial reweighting (ARL), knowledge distillation (KD), Graph of Gradients (GoG), and *Reckoner* as our baselines for comparison in this study.

### 2.3 Subgroup-oriented Fairness

Beyond methods that rely on explicit demographics or avoid them entirely, a growing line of work targets subgroup-oriented fairness by enforcing equity across diverse population partitions. However, Kearns et al. [45] showed that optimizing fairness for a small set of protected groups can yield “fairness gerrymandering,” where other subgroups suffer large disparities. Hébert-Johnson et al. [31] addressed this via multicalibration, enforcing predictive calibration across broad subgroup families.

Another related line of research focuses on achieving equitable subgroup performance through distributionally robust optimization (DRO). Given access to group annotations, these methods aim to *minimize the worst-case subgroup error*. For example, Group DRO (Group Distributionally Robust Optimization) [75] achieves this by dynamically adjusting the training objective to focus on the groups with the highest loss. Building on this, Liu et al. [58] proposed Just Train Twice (JTT), which removes the need for explicit group labels by first using a baseline model to identify high-loss or misclassified samples as latent hard subgroups, then retraining a new model that upweights these samples to boost performance on the worst-performing groups.

Despite gains, two limits remain: (i) dependence on predefined or proxy groupings that may be unavailable or too coarse for fine-grained heterogeneity, and (ii) objectives centered on the worst group, leaving non-worst disparities unresolved. However, in practical settings, subgroup gaps often persist even when average or worst-group accuracy improves [48].

Additionally, Sohoni et al. [78] investigated *hidden stratification*, where a single class label conceals multiple unlabeled subclasses with varying difficulty. Their approach clusters data *within each class* to identify these subclasses and then applies Group-DRO to optimize the worst-case subclass accuracy. The clustering is strictly class-conditional—each subclass remains tied to its original class—and the objective is to improve within-class robustness. In contrast, our work does not operate through class-conditioned subclass formation. We examine model behavior using latent, class-agnostic clusters that capture variations in representation and sensitivity, allowing ethically constrained fairness evaluation beyond demographics and class-specific partitions.

## 2.4 Ethical AI in healthcare and aligning with human-centered modeling

Ethical AI in healthcare centers on four principles: *beneficence* (promote patient well-being), *non-maleficence* (avoid foreseeable harm), *justice* (ensure equitable treatment across groups), and *autonomy* (enable informed, voluntary choices) [8, 23, 36]. These principles are echoed across international AI ethics guidelines and form a shared foundation for trustworthy AI [19, 41]. However, principles alone are insufficient—they must be translated into practical design and evaluation steps for real-world systems [65]. In healthcare, where AI models are incrementally influencing patient outcomes and clinical decisions, such alignment with human-centered modeling becomes critical. Particularly:

- *Beneficence* emphasizes the obligation to design and implement systems that actively promote overall well-being and deliver measurable improvements [82].
- *Non-maleficence* focuses on minimizing risks and preventing harm, supported by frameworks that identify and mitigate potential harms throughout the machine learning lifecycle [82].
- *Justice* requires that algorithms perform equitably across diverse populations, avoiding systematic disadvantages to specific subgroups [41].
- *Autonomy* promotes consistent and stable model behavior, enabling users to rely on AI outcomes and making informed decision-making in line with ethical standards [19, 38, 65].

These principles anchor ethical AI in human-centered computing, ensuring that technical performance is balanced with fairness, safety, and trustworthiness.

## 2.5 Ethical AI vs fairness

While fairness has become one of the most prominent concerns in machine learning, it represents only one dimension of ethical AI [26]. Fairness typically refers to the equitable treatment of individuals or subgroups, often quantified through statistical metrics across groups [22, 28]. These measures address the principle of *justice*, ensuring that no population is disproportionately disadvantaged by algorithmic predictions.

However, this narrow focus creates a gap between fairness as currently defined in machine learning and the broader requirements of ethical AI, a concern raised in recent ethical AI literature [6, 15, 18, 77, 86]. Principles such as *beneficence* and *non-maleficence* demand that systems not only avoid disparities but also improve outcomes while causing no harm for any subgroup [8]. *Autonomy* requires consistency so that users can rely on the AI system. Yet, these dimensions are rarely embedded into fairness frameworks, leaving critical ethical concerns unaddressed.

Such a gap is particularly critical to address in healthcare, where fairness is necessary but not sufficient [41]: predictive models must not only perform equitably across patients but also improve health outcomes, avoid harmful decisions, and support trustworthiness.

*To the best of our knowledge, no prior work has jointly operationalized fairness and core ethical principles in model development.* This paper directly tackles the above-discussed gaps—advancing the goal of ethical fairness in human-centered AI. In the absence of established ethical fairness baselines, we consider state-of-the-art (SoTA) fairness-without-demographics (FWD) approaches as baselines.

## 3 Fairness Metrics

Although fairness is a major focus in machine learning, no existing metric adequately captures the broader scope of ethical fairness [13]. This section reviews the commonly used fairness metrics and then introduces a new framework for comprehensive ethical fairness evaluation, aligning fairness assessment more closely with the core principles of ethical AI.

### 3.1 Limitations of existing fairness metrics

Fairness in machine learning is typically assessed using statistical measures that quantify disparities in model outcomes across protected groups. Common binary metrics include Demographic Parity (DP)—which measures whether positive prediction rates are equal across subgroups—and Equal Opportunity Difference (EOD), which compares true positive rates to ensure equitable treatment [22, 28, 101].

However, these binary metrics capture only pairwise group differences (e.g., male vs. female) and fail to reflect disparities across multiple subgroups. To overcome this limitation, multi-group extensions such as generalized EOD [69] and Relative Disparity (RD) [3] have been introduced. These metrics aggregate performance gaps across all subgroups to provide a broader view of fairness. For instance, RD measures the ratio between the best- and worst-performing subgroups (e.g., by recall or F1-score), with values closer to 1 indicating greater equity.

Despite these advances, these metrics still fall short in key ways. Metrics that rely solely on aggregated performance (e.g., overall accuracy or AUC) or extreme-value summaries (e.g., max–min ratios) can obscure systematic harm—masking whether certain subgroups consistently underperform [29, 45, 75]. A model may achieve parity in statistical terms yet still produce outcomes that disproportionately burden specific populations, conflicting with the ethical principles of *justice* and *non-maleficence*. Moreover, existing fairness metrics do not assess whether model improvements benefit all subgroups and the overall population. They equalize outcomes without ensuring collective efficacy, overlooking the ethical principle of *beneficence*.

### 3.2 BHE: Fairness Metrics Aligned with Bioethics

To bridge the gap between technical fairness and ethical accountability, we introduce the **BHE Metrics** (*Benefit, Harm-Avoidance, Equity*), derived from known-demographic-wise F1-scores, such as age, sex, sensor, disorder scores like PhQ10, and more, aggregated across  $N$  folds. Moreover, each fold’s test set is person-disjoint from the others, and together they encompass the entire population, ensuring a comprehensive and unbiased evaluation. Notably, demographic information is used exclusively during evaluation; during model training, no demographic information is used.

To meaningfully evaluate whether **FLARE** enhances ethical fairness, it is essential to use datasets that include known demographic or sensitive attribute labels. Such datasets provide the necessary ground truth for quantifying ethical principles and fairness across defined subgroups and verifying whether **FLARE** can indeed promote ethically constrained equitable outcomes. However, most human-centered datasets lack this information, making direct fairness evaluation challenging. Therefore, demonstrating consistent ethical fairness improvements on datasets with available demographic annotations, leveraged in this paper for evaluation, serves as a proxy validation—establishing confidence that **FLARE** can generalize ethical fairness across broader human-centered applications and domains where demographic data are unavailable or impractical to collect.

BHE metrics compare the fair solutions (**FLARE** and other fair AI approaches) with SoTA benign baseline approaches, and measure the changes in ethical principles, outlined below:

Let  $\mathcal{S}$  denote the set of all demographic subgroups, and  $F1_s^m(\theta)$  the F1-score of model  $m$  ( $m \in \{\mathbf{FLARE}, \mathbf{Base}\}$ ) on subgroup  $s$ . We define the BHE deltas  $\Delta$  as follows:

$$\Delta B = \frac{1}{|\mathcal{S}|} \sum_{s \in \mathcal{S}} (F1_s^{\mathbf{FLARE}}(\theta)) - \frac{1}{|\mathcal{S}|} \sum_{s \in \mathcal{S}} (F1_s^{\mathbf{Base}}(\theta)), \quad \Delta H = \min_{s \in \mathcal{S}} (F1_s^{\mathbf{FLARE}}(\theta) - F1_s^{\mathbf{Base}}(\theta)),$$

$$\Delta E = \text{Std}(\{F1_s^{\mathbf{Base}}(\theta)\}_{s \in \mathcal{S}}) - \text{Std}(\{F1_s^{\mathbf{FLARE}}(\theta)\}_{s \in \mathcal{S}}).$$

- **Benefit** ( $\Delta B$ ): Reflects the change in average predictive performance across subgroups, corresponding to the ethical principle of *beneficence*—higher  $\Delta B$  promotes the greatest overall benefit to the population [36].
- **Harm-Avoidance** ( $\Delta H$ ): Captures the smallest subgroup-level improvement, emphasizing protection against systematic disadvantage and embodying *non-maleficence*—the obligation to avoid harm [8]. By

taking the minimum subgroup-wise F1 improvement (which can be negative according to the equation-indicating harm),  $\Delta H$  ensures that even the most vulnerable subgroup is considered; when  $\Delta H \geq 0$ , no subgroup experiences a decline in performance, thereby guaranteeing that the model does not introduce harm to any population segment, adhering to *non-maleficence* principle.

- **Equity ( $\Delta E$ ):** Quantifies the reduction in performance variability across subgroups—typically expressed as a lower standard deviation of model accuracy or outcomes among demographic categories. A lower standard deviation indicates that the AI system performs consistently and reliably across diverse populations, ensuring that no group is systematically advantaged or disadvantaged [11]. This uniformity of performance embodies a commitment to *justice*, as it upholds fairness and equal treatment in decision-making. At the same time, it reinforces *autonomy*, since consistent model behavior enhance stability i.e. reliable decision making [12, 23]. Reliable and equitable outputs reduce uncertainty, build confidence in human oversight, and preserve meaningful human control—core elements of *autonomy* in the WHO’s ethical framework for AI in health[44].

Higher  $\Delta B$  and  $\Delta H$  indicate greater benefit and stronger safeguards for vulnerable subgroups, corresponding to *goals-i and -iii* in Section 1. Similarly, a higher  $\Delta E$  (reflecting reduced disparity) signifies improved equity and stability, aligning with *goals-ii* in Section 1.

This formulation ensures that, for all three metrics, larger positive  $\Delta$  values consistently represent ethically superior outcomes—enhanced collective utility, minimized harm to disadvantaged groups, and diminished disparities in model performance.

#### 4 Design Choice

**Optimization theory background that supports FLARE.** Fairness in machine learning can be examined through the geometry of optimization. Specifically, the Hessian matrix of the loss function provides insights into the curvature of the loss landscape, where sharp minima—characterized by a large top eigenvalue of the Hessian—indicate higher sensitivity to parameter perturbations and instability in generalization [17, 39]. Recent work has shown that subgroups associated with sharper regions in the loss surface tend to lie closer to the model’s decision boundaries. As a result, these groups experience less stable and less accurate model performance than others. This finding suggests that curvature disparities, as captured by the top eigenvalue of the Hessian of the loss, can serve as a useful proxy for identifying fairness gaps across demographic subgroups [84].

Since computing the full Hessian is computationally prohibitive in high-dimensional models, following the literature [51, 83, 96], we adopt Fisher information as a tractable surrogate to measure the model’s loss-landscape curvature. Under standard regularity conditions, the Fisher information matrix (FIM) coincides with the expected Hessian of the negative log-likelihood [62], capturing similar curvature characteristics in a more scalable form.

Consequently, a lower top eigenvalue of the FIM reflects flatter minima and smoother curvature—implying greater generalizability [57, 97], as the model’s decisions remain *stable* across unseen or noisy conditions. Moreover, when FIM disparities across subgroups are reduced, the model achieves more uniform curvature and decision-boundary distances among groups, promoting robustness and *fairness* through consistent decision boundaries across subgroups.

Building on these insights, **FLARE** unifies Fisher-based curvature information, loss dynamics, and embedding-space structure to reveal latent subgroups that exhibit disproportionate model performance. By identifying these hidden disparities, **FLARE** guides optimization toward flatter and more equitable loss landscapes across the discovered subgroups. This promotes fairness without relying on demographic attributes (FWD), while enhancing generalizability through improved model stability—thereby advancing the ethical principles of *justice and autonomy*. Simultaneously, **FLARE** enhances overall model efficacy without compromising any subgroup’s

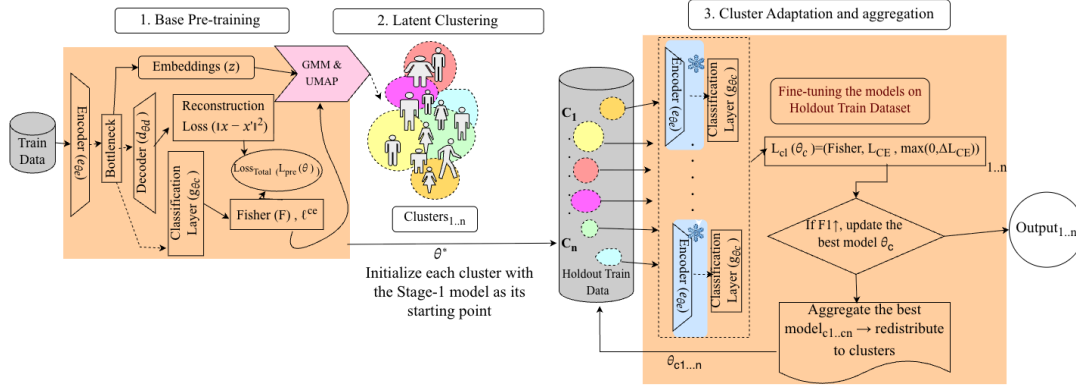


Fig. 1. Proposed Approach: (1) Base pre-training learns embeddings with Fisher penalty regularization, (2) UMAP+GMM clustering captures behavior-based similarity, and (3) cluster models are fine-tuned and aggregated with stability constraints

performance, balancing collective improvement with individual protection in line with the principles of *beneficence* (promoting good) and *non-maleficence* (preventing harm).

**FLARE**'s design choices comprise three modules shown in Figure 1, and discussed below:

#### 4.1 Base pretraining.

As we can see from Figure 1 (step 1), the first module involves training an encoder–decoder–classifier framework ( $e_{\theta_e}, d_{\theta_d}, g_{\theta_c}$ ) to learn model-behavior-aware comprehensive representations of the data. Given an input sample  $x$  with ground-truth label  $y$ , the encoder  $e_{\theta_e}$  maps the input into a latent representation  $z = e_{\theta_e}(x)$ . The classifier  $g_{\theta_c}$  produces a label prediction  $\hat{y} = g_{\theta_c}(z)$  from the latent code, while the decoder  $d_{\theta_d}$  reconstructs the input as  $\tilde{x} = d_{\theta_d}(z)$ . The classifier is trained using a joint objective that balances reconstruction, classification, and stability:

$$\mathcal{L}_{\text{pre}}(\theta) = (1 - \alpha) \|x - \tilde{x}\|_2^2 + \alpha \left( \beta \ell_{\text{CE}}(\hat{y}, y) + (1 - \beta) F(x, y; \theta) \mathbb{I}\{\hat{y} = y\} \right). \quad (1)$$

Here: the first term,  $\|x - \tilde{x}\|_2^2$  is the mean-squared error (MSE) reconstruction loss, encouraging the latent representation  $z$  to retain as much information from  $x$  as possible.  $\ell_{\text{CE}}(\hat{y}, y)$  is the cross-entropy loss between the predicted label  $\hat{y}$  and the true label  $y$ , which drives the model to make accurate classifications. And,  $F(x, y; \theta)$  denotes Fisher penalty, i.e., promoting reduction of the top eigenvalue of the FIM, which measures the sensitivity of the model's loss around correctly classified samples [55]. Minimizing this term reduces the local curvature of the loss landscape, encouraging the model to converge toward flatter minima, which correspond to more stable generalization behavior, thereby enhancing *autonomy*.  $\mathbb{I}\{\hat{y} = y\}$  is an indicator function that equals 1 if the sample is classified correctly and 0 otherwise, ensuring that Fisher penalty regularization is applied only to correctly predicted samples. This training avoids penalizing the curvature of misclassified samples, since they are already penalized to encourage crossing the decision boundaries via the  $\ell_{\text{CE}}(\hat{y}, y)$  loss.  $\alpha \in [0, 1]$  balances reconstruction against supervised objectives.  $\beta \in [0, 1]$  controls the trade-off between classification accuracy (cross-entropy) and stability (Fisher penalty) within the supervised component.

In this module, intuitively, minimizing the Fisher Penalty across all samples lowers its overall upper bound and variance, aligning curvature more evenly throughout the population. As discussed above, equitable loss-landscape curvature promotes fair predictions across inputs, thereby enhancing *justice*. Thus, this curvature regularization acts as a fairness-promoting mechanism, improving *justice* and *autonomy* of the base-pretrained model  $\theta^*$ 's predictions without requiring access to sensitive demographic attributes.

However, as prior work on fairness without demographics has shown (discussed in Section 2.2), enforcing such uniform regularization globally can yield suboptimal results—since it fails to capture nuanced differences in how the model interacts with diverse subgroups [14, 49]. To overcome these limitations, our encoder–decoder design in the pretraining module explicitly structures the model to differentiate samples based on both representational and model behavioral similarity. The encoder captures latent features, i.e., embeddings that reveal which samples share similar representational structure—meaning the model is likely to apply similar decision rules to them. Simultaneously, the classifier’s cross-entropy loss captures each sample’s classification efficacy (how confidently it is predicted), while the Fisher penalty captures each sample’s sensitivity to perturbation and its proximity to the decision boundary. Together, these metrics characterize the model’s behavior for each data point, which informs the following module to identify latent subgroups that experience disproportionate model treatment and, through the last module, attain latent subgroup-guided optimization to promote ethical fairness.

## 4.2 Latent Clustering

Building upon the baseline model  $\theta^*$ ’s behavior-informed representations learned during pretraining, this module seeks to reveal hidden stratification—that is, differences in model treatment (i.e., performance and behavior) across latent subgroups that are not explicitly defined by demographic attributes. While the pretraining module encourages flatter loss surfaces and wider decision margins globally, such uniform regularization may mask local disparities: some samples may still reside near sharper regions of the loss landscape, corresponding to smaller decision boundary margins and higher predictive uncertainty. To uncover these disparities, we perform model behavioral clustering, grouping samples not only by how they are represented in the latent space but also by how the model  $\theta^*$ ’s loss landscape behaves around them.

For each input  $x$  with label  $y$ : we form a vector  $s = [z, \ell^{\text{CE}}, F]$ , where  $z = e_{\theta_e}(x)$  is the encoder embedding,  $\ell^{\text{CE}} = \ell_{\text{CE}}(\hat{y}, y)$  is the cross-entropy loss, and  $F$  is the Fisher penalty around this input.

To form coherent behavioral clusters, we first employ Uniform Manifold Approximation and Projection (UMAP) [30] to reduce  $s$  to a lower dimension, followed by a Gaussian Mixture Model (GMM) [74] that partitions samples into  $C$  clusters, with  $C$  chosen to avoid degenerate (empty) groups. This approach yields clusters reflecting *behavioral similarity* under the model, not just raw input features. Each cluster thus represents a group of samples that are similar in both their feature representation and the model’s local loss landscape curvature and efficacy, effectively defining behaviorally homogeneous subgroups. Importantly, this clustering is performed at the sample level, not at the individual or demographic level. As a result, multiple samples from the same subject can belong to different clusters depending on how the model’s decision geometry interacts with each instance. This property is critical for identifying subtle, data-driven fairness gaps that demographic-based methods may overlook.

In essence, this module reframes ethical fairness as a loss landscape analysis problem. By grouping samples based on their shared curvature characteristics, classification dynamics, and representational traits, it identifies latent subgroups that differ systematically in model efficacy, robustness, stability, or margin distance. These behaviorally coherent clusters expose where the model performs inconsistently, providing a principled basis for targeted adaptation promoting ethically guided fairness attainment in the subsequent module. Throughout the rest of the paper, identified clusters will be used synonymously with latent subgroups.

## 4.3 Cluster-specific Adaptation and Aggregation

After revealing latent subgroups through curvature- and behavior-aware clustering, this module of **FLARE** focuses on ethically fair adaptation. It ensures that each cluster, i.e., latent subgroup, receives tailored optimization that respects both performance equity and ethical constraints. This section’s training is performed on a disjoint hold-out dataset from the prior modules, ensuring unbiased model optimization.

**4.3.1 Cluster Adaptation:** Once clusters are identified, we specialize models for each cluster  $c$  by adapting the pretrained model  $\theta^*$ . The early encoder layers are frozen to preserve generic knowledge learned during pretraining, while the later encoder and classifier parameters are fine-tuned to capture cluster-specific patterns. This hierarchical adaptation enables *localized fairness correction* without sacrificing generalizability.

The training objective for cluster  $c$  specific model is

$$\mathcal{L}_{cl}(\theta_c) = \alpha \times \underbrace{\ell_{CE}(\hat{y}, y)}_{\text{accuracy}} + (1 - \alpha) \times \underbrace{F(x, y; \theta_c)}_{\text{stability on corrects}} + \underbrace{\max\{\ell_{CE}(\hat{y}, y) - \ell_{CE}^{pre}, 0\}}_{\text{do-no-harm vs. baseline}}. \quad (2)$$

Here:  $\ell_{CE}(\hat{y}, y)$  is the cross-entropy loss between the prediction  $\hat{y}$  and the ground truth  $y$ , measuring classification error.  $F(x, y; \theta_c)$  is the Fisher penalty under  $\theta_c$ , quantifying sensitivity of the model to parameter perturbations specific to cluster  $c$  samples, encouraging flatter minima and improving decision boundary margins within each cluster. Similar to Section 4.1, Fisher penalty is computed *only on correctly classified samples*, ensuring that curvature smoothing focuses on reliable decision regions, while misclassified samples are handled through the cross-entropy term that encourages boundary correction. This separation promotes accuracy and stability for the correct samples, promoting *beneficence and autonomy*, while preventing enhancement of stability of misclassified samples, promoting *non-maleficence*. Moreover, just as in Section 4.1, lowering the Fisher penalty promotes more uniform curvature—yielding fairer, more consistent performance across cluster  $c$  samples, promoting *justice*.

Given,  $\ell_{CE}^{pre}$  is the cross-entropy loss of the cluster  $c$  samples under the pretrained model  $\theta^*$ , the term  $\max\{\ell_{CE}(\hat{y}, y) - \ell_{CE}^{pre}, 0\}$  represents a “do-no-harm” regularizer. It is positive only if the cluster-specific model performs worse than the pretrained baseline  $\theta^*$ , preventing harmful updates, promoting *non-maleficence*; if the performance is improving, this term vanishes. Additionally,  $\alpha \in [0, 1]$  balances accuracy (cross-entropy) against stability and fairness (Fisher regularization).

Through this design, each cluster-specific model evolves within a locally fairer loss geometry, improving efficacy for underperforming subgroups while safeguarding others from degradation.

**4.3.2 Aggregation:** While local adaptation refines each subgroup, independent optimization can cause clusters to drift apart, creating uneven decision geometries and potentially new disparities. To counter this, **FLARE** introduces a periodic running-average aggregation mechanism that promotes equilibrium across clusters, ensuring that improvements remain shared and harmonized.

At scheduled intervals, parameters from all cluster-specific models are aggregated through a running mean:

$$\bar{\theta} = \frac{1}{C} \sum_{c=1}^C \theta_c,$$

where  $C$  denotes the number of clusters and  $\theta_c$  the parameter vector associated with cluster  $c$ .

The aggregated model  $\bar{\theta}$  represents a consensus parameterization, capturing shared curvature and decision geometry across subgroups [27, 37, 102]. It is then redistributed to all clusters, serving as a synchronized initialization for subsequent adaptation. Each cluster evaluates whether adopting  $\bar{\theta}$  improves its own validation F1 score. If the update yields improvement,  $\bar{\theta}$  replaces the prior model; otherwise, the cluster retains its previous parameters.

Formally, the best model for cluster  $c$ , upon each aggregation step is defined as:  $\theta_c^* = \arg \max_{\theta_c, \bar{\theta}} F1_{val}(D_c)$ , where  $D_c$  represents cluster  $c$ 's data distribution, sampled from its validation set. This procedure balances knowledge sharing [81] and specialization [33]: clusters benefit from collective information through  $\bar{\theta}$  while retaining the ability to reject it if it degrades local performance. By comparing the validation F1 scores between  $\bar{\theta}$  and the previous cluster model  $\theta_c$ , each cluster effectively performs a local *model selection step* that guards against utility drop, promoting *non-maleficence*.

The final system is given by  $\{\theta_c^*\}_{c=1}^C$ , ensuring that each cluster settles on the parameter configuration—either its adapted version or the aggregated one—that maximizes its local validation performance. Overall, by coupling local specialization with global reconciliation, the model converges toward a fair curvature across subgroups—flatter, more robust, and more equitable in its decision geometry—while adhering to ethical constraints.

## 5 Approach

Following the design principles described in Section 4, **FLARE** operationalizes the proposed framework through two main algorithmic steps: (Algorithm 1 - modules 1,2) *Base Pretraining and Latent Clustering*, and (Algorithm 2 - module 3) *Cluster-specific Adaptation and Aggregation*. These algorithmic steps correspond directly to the components illustrated in Figure 1, where Module 1 and 2 produce Fisher-regularized embeddings and behaviorally meaningful clusters, and Module 3 refines model performance on those clusters through stability-aware adaptation.

### 5.1 Algorithm 1 – Modules 1,2: Base Pretraining and Latent Clustering

---

#### Algorithm 1 Modules 1–2: Base Pretraining and Latent Clustering

---

**Require:** Fold  $k \in \{1, \dots, K\}$  with train+holdout train (80%/20%) and person-disjoint test; hyperparameters  $\alpha, \beta, \eta, E, C$ .

- 1: Initialize encoder–decoder–classifier  $M_\theta$ .
- 2: **for** epoch = 1 to  $E$  **do**
- 3:   **for** each batch  $(x, y) \in \text{train}$  **do**
- 4:      $(z, \tilde{x}, \hat{y}) \leftarrow M(x)$  ▷ Forward pass: embeddings, reconstruction, predictions
- 5:     Compute Fisher penalty  $F_c$  for correctly classified samples only.
- 6:      $\mathcal{L}_{\text{pre}} \leftarrow (1 - \alpha)\|x - \tilde{x}\|_2^2 + \alpha[\beta\ell_{\text{CE}}(\hat{y}, y) + (1 - \beta)F_c]$
- 7:      $\theta \leftarrow \theta - \eta \nabla_{\theta} \mathcal{L}_{\text{pre}}$  ▷ Parameter update
- 8:   **end for**
- 9:   Evaluate on test; save  $\theta^*$  if validation improves.
- 10: **end for**
- 11: **Feature Extraction:** Using  $\theta^*$ , compute  $(z, \ell_{\text{CE}}, F)$  for all samples.
- 12: Combine descriptors  $s = [z, \ell_{\text{CE}}, F]$  into sets  $S_{\text{corr}}$  (correct) and  $S_{\text{all}}$ .
- 13: **Clustering:** Fit UMAP  $\varphi$  on  $S_{\text{corr}}$ ; train GMM( $C$ ) on  $\varphi(S_{\text{corr}})$ .
- 14: Assign cluster IDs to all samples using GMM posterior probabilities.

**Ensure:** Checkpoint  $\theta^*$ , UMAP  $\varphi$ , GMM model, and cluster assignments.

---

Module 1 trains an encoder–decoder–classifier network using the Fisher-regularized composite loss introduced earlier. The objective balances reconstruction fidelity, predictive accuracy, and curvature regularization. During training (Lines 3–10 in Algorithm 1), each batch is passed through the encoder to obtain latent representations  $z$ , reconstructed outputs  $\tilde{x}$ , and class predictions  $\hat{y}$ . Fisher penalty is computed only for correctly classified samples and combined with the reconstruction and classification losses to form the total objective. After every epoch (Line 11), model performance on the person-disjoint test set is evaluated, and the best-performing checkpoint  $\theta^*$  is retained for downstream clustering.

Using  $\theta^*$ , we extract three descriptors for each sample: latent embedding ( $z$ ), cross-entropy loss ( $\ell_{\text{CE}}$ ), and Fisher penalty ( $F$ ). These features are combined to form a joint representation  $s = [z, \ell_{\text{CE}}, F]$ . In Module 2 (Lines 17–20), UMAP is applied to the correctly classified subset to preserve local geometry in a lower-dimensional manifold. A Gaussian Mixture Model (GMM) is then fitted on this manifold to partition the samples into  $C$  clusters. Finally, each sample is assigned a cluster label based on its GMM posterior probability. Module 1 ensures the encoder

learns comprehensive embeddings, while Module 2 identifies latent model-behavioral-wise clusters based on geometry, loss dynamics, and curvature sensitivity.

## 5.2 Algorithm 2 - Module 3: Cluster-specific Adaptation and Aggregation

---

### Algorithm 2 Module 3: Cluster-specific Adaptation and Conditional Aggregation

---

```

1: Inputs: pretrained  $\theta^*$ ; clusters  $\{\mathcal{D}_{\text{train2}}^c, \mathcal{D}_{\text{val}}^c, \mathcal{D}_{\text{test}}^c\}_{c=1}^C$ ; freeze depth  $L$ ; weights  $\alpha, \lambda$ ; lr  $\eta$ ; epochs  $E$ ; aggregation
   interval  $\tau$ .
2: Initialize  $\theta_c \leftarrow \theta^*$ ; freeze first  $L$  encoder layers for all  $c$ .
3: Set  $\text{bestF1}^{(c)} \leftarrow -\infty$  for each cluster.
4: for epoch = 1 to  $E$  do
5:   for  $c = 1$  to  $C$  do
6:     for mini-batch  $(x, y) \subset \mathcal{D}_{\text{train2}}^c$  do
7:        $\hat{y} \leftarrow M_{\theta_c}(x), \hat{y}^* \leftarrow M_{\theta^*}(x)$ 
8:       Compute CE,  $\text{CE}^*$ , and F; apply F only on correct samples.
9:       Compute loss:  $\mathcal{L}_{\text{cl}} = \alpha \text{CE} + (1 - \alpha)F + \lambda[\text{CE} - \text{CE}^*]_+$ 
10:       $\theta_c \leftarrow \theta_c - \eta \nabla_{\theta_c} \mathcal{L}_{\text{cl}}$ 
11:     end for
12:     Evaluate  $\text{F1}_{\text{val}}^{(c)}$ ; if improved, save best checkpoint.
13:   end for
14:   if epoch mod  $\tau = 0$  then
15:      $\bar{\theta} \leftarrow \frac{1}{C} \sum_{c=1}^C \theta_c$  ▷ Compute running average
16:     for  $c = 1$  to  $C$  do
17:       Evaluate  $\bar{\theta}$  on  $\mathcal{D}_{\text{val}}^c$ ; if  $\text{F1}_{\text{val}}^{(c)}(\bar{\theta}) > \text{F1}_{\text{val}}^{(c)}(\theta_c)$ , set  $\theta_c \leftarrow \bar{\theta}$ 
18:     end for
19:   end if
20:   Stop when  $\frac{1}{C} \sum_{c=1}^C \text{F1}_{\text{val}}^{(c)}$  converges. ▷ Early stopping
21: end for
22: for  $c = 1$  to  $C$  do
23:   Reload best checkpoint  $\theta_c^*$  and evaluate on  $\mathcal{D}_{\text{test}}^c$ .
24: end for

```

---

Module 3 fine-tunes cluster-specific models and performs conditional aggregation to achieve a balance between local specialization and global stability. Each cluster model is initialized from the shared checkpoint  $\theta^*$  and partially frozen (Line 2 in Algorithm 2) to retain domain-invariant generic structure learned during pretraining.

This module is trained on the holdout training split to prevent overfitting and ensure that adaptation remains generalizable across participants and clusters. Fine-tuning proceeds (Lines 5–12) with the cluster-specific objective  $\mathcal{L}_{\text{cl}}$  defined in Section 4, which integrates accuracy, Fisher-based stability, and the one-sided “do-no-harm” constraint. Fisher penalty terms are again computed only on correctly classified samples. Validation F1 scores are tracked per cluster (Line 13), and the best-performing checkpoint is saved.

To maintain coherence across clusters, periodic aggregation is applied every  $\tau$  epochs (Lines 15–23). The average model  $\bar{\theta} = \frac{1}{C} \sum_{c=1}^C \theta_c$  is computed and *offered* to all clusters. Each cluster  $c$  tests  $\bar{\theta}$  on its validation data; if adopting  $\bar{\theta}$  improves validation F1, the cluster updates its parameters; otherwise, it continues training with its own  $\theta_c$ . This conditional aggregation (Lines 18–21) enables positive transfer between clusters while preventing negative interference. Early stopping (Line 24) is triggered when the mean validation F1 across all clusters

stabilizes, ensuring convergence to balanced, stable solutions. Finally, each cluster reloads its best checkpoint for testing (Lines 26–27), and the ensemble  $\{\theta_c^*\}_{c=1}^C$  forms the final output.

Module 3 refines each cluster’s model through targeted, Fisher-regularized adaptation while ensuring fairness and stability via the “do-no-harm” constraint and conditional aggregation. The resulting ensemble preserves global robustness while allowing local specialization, achieving fairness without demographic supervision.

## 6 Experimental Results

This section evaluates **FLARE** to assess its ability to enhance ethical fairness without relying on explicit demographic or sensitive attribute information, while maintaining high predictive accuracy across diverse behavioral and physiological sensing tasks. We begin by describing the datasets and model configurations. Next, we assess the effectiveness of **FLARE**. Finally, we provide an empirical validation of the design choices.

### 6.1 Datasets and Models

**FLARE** is tested on three multimodal datasets: **OhioT1DM** [61]—continuous glucose and insulin pump data from 11 participants (normal vs. hyperglycemia, processed per [10]); **Intern Health Study (IHS)** [1]—a 14-month study of 85 medical interns combining PHQ-9 scores, daily mood, and Fitbit-derived features, labels are derived from mood thresholds (>8 positive, <3 negative) in line with [60]; and **Electrodermal Activity (EDA)** [90, 91]—multimodal physiological signals (EDA, HR, ACC, TEMP, HRV) from 76 participants with 340 handcrafted features for stress detection.

*Known Demographics for Evaluating Subgroup-wise Ethical Fairness through BHE Metrics.* For **OhioT1DM** [61], we evaluate along attributes reported in the dataset and prior work, including *Sex* (male/female), *Age* (20–40, 40–60, 60–80), *insulin Pump and Model* (e.g., 530G, 630G), *Sensor Band* (Empatica, Basis), and *Cohort* (2018 vs. 2020); data processing follows Appendix 2.4 of [10]. For **EDA** [90, 91], we assess *BHE Metrics* across *Medication and disorder Groups* (control/pre-dose/post-dose) and *Sex*. For **IHS** [1], available *BHE Metrics* evaluation attributes include *Sex, Age, Ethnicity, Residency Specialty* (12+ categories), and a baseline mental-health indicator  $PHQ10 > 0$ .

*Evaluation Setup.* All datasets use an  $N$ -fold evaluation setup in which the train and test sets are person-disjoint within each fold. The training participants are further divided 80:20 into `train` and `holdout-train` subsets. The `train` split is used for pretrained classifier training and clustering (Sections 4.1 and 4.2), while the `holdout-train` split supports Cluster-specific Adaptation and Aggregation (Section 4.3). As noted in Section 3.2, each fold’s test set is mutually exclusive and collectively spans the entire population, ensuring a comprehensive and unbiased evaluation. The configuration of folds across datasets is as follows: **IHS**: 5 folds with 17 users in test set per fold. **EDA**: 4 folds with 19 users in the test set per fold. **OhioT1DM**: 4 folds with test sets containing 3, 3, 2, and 3 users, respectively.

*Models.* Each dataset employs an autoencoder–classifier backbone tailored to its feature dimensionality and domain characteristics. Specifically, DNN model (used for **OHIO-T1DM**) consists of a 256–128–64–32 encoder and a 32–8–2 classifier head. The DNN model (for **IHS**) follows a compact 128–64–32 encoder with a 32–16–8–2 classifier. For **EDA** DNN model, the encoder compresses the input into a 128-dimensional latent representation using three linear layers with a deeper 128–64–64–2 classifier. Each model integrates a symmetric decoder for reconstruction learning, enabling joint representation regularization. These ‘pretrained autoencoder–classifier’ networks (from module 1 in Section 4.1) serve as the initialization stage for **FLARE**, on which it performs cluster-specific adaptation and cross-cluster aggregation.

*Benign Baseline Models.* The *benign baseline* refers to standard supervised models trained without fairness or ethical regularization, serving as reference points for evaluating the BHE metrics of **FLARE** and other FWD

approaches. These baselines adopt established architectures and hyperparameter configurations from prior work. For the **OhioT1DM** dataset, we followed the models and parameter settings of Marling and Bunescu [61] and Arefeen and Ghasemzadeh [10]. For the **EDA** dataset, we implemented the configurations proposed by Xiao et al. [90, 91]. For the **IHS** dataset, since model configuration was not provided in the literature [1], the baseline was optimized through a combination of *Optuna* [76] hyperparameter tuning and iterative manual refinement to obtain the highest benign performance.

*Hyperparameter Optimization.* To ensure optimal and reproducible performance, all hyperparameters—including learning rate, batch size, weight decay, and the regularization coefficients  $\alpha$ ,  $\beta$ , and  $\gamma$ —are tuned using the *Optuna* hyperparameter optimization framework. Optuna employs Bayesian optimization with early stopping and dynamic pruning to efficiently explore the search space, automatically selecting the configuration that maximizes validation performance while maintaining fairness and stability objectives [16]. Comprehensive architectural, training, and preprocessing specifications are detailed in Appendix A.1.

## 6.2 Evaluation of **FLARE**'s Effectiveness

We evaluate the ethical fairness of **FLARE** through a multi-stage analysis. First, we assess its *Beneficence*—both overall and across demographic subgroups—by comparing performance against a benign baseline and recent state-of-the-art *fairness-without-demographics (FWD)* models. Next, we conduct comprehensive **BHE evaluation** to compare **FLARE** with the same SoTA FWD baselines, quantifying its relative advantages in achieving balanced improvements across ethical dimensions. Finally, we empirically validate two core ethical properties of **FLARE**: its ability to achieve *user-level autonomy*, enabling consistent behaviour across users, promoting stability; and its adherence to the *Do No Harm* principle, ensuring that adaptation never reduces performance while promoting fairness across the population.

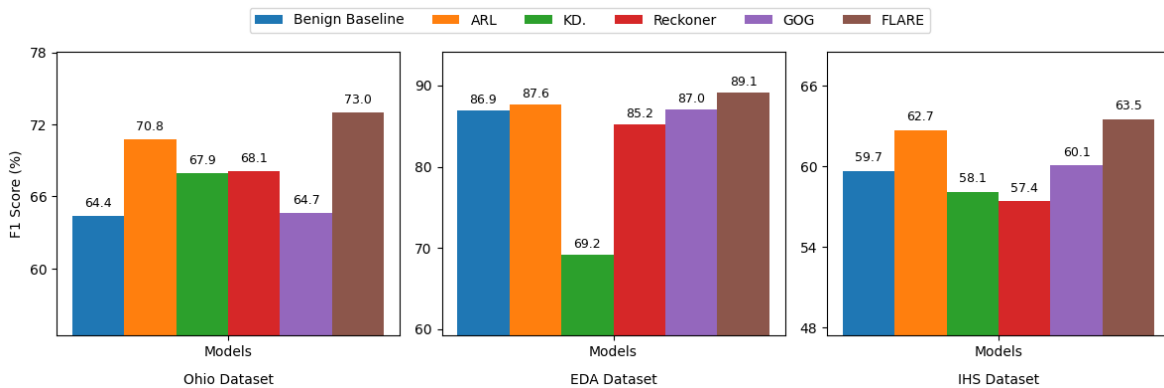


Fig. 2. Overall F1-scores across all models for each dataset.

**6.2.1 Beneficence Comparison for Baselines vs. FLARE.** *Beneficence* is a core principle of ethical AI, emphasizing the enhancement of overall well-being through improved model performance. Therefore, any decline in predictive performance—either overall or across subgroups—when using **FLARE** compared to baselines would contradict this principle. To assess *beneficence*, we compare the proposed **FLARE** model with the Benign Baseline and four representative SoTA FWD baselines—Adversarial Reweighting Learning (ARL) [49], Knowledge Distillation (KD) [14], Reckoner [68], and Graph of Gradients (GoG) [59]. These methods capture distinct paradigms of fairness optimization, as discussed in Section 2.2.

**Figure 2** shows the overall F1-scores for all models across datasets. **FLARE** consistently achieves the highest performance—**73.0%** on the OhioT1DM dataset, **89.1%** on EDA, and **63.5%** on IHS—demonstrating that its optimization strategy enhances predictive quality, ensuring *beneficence*. ARL attains competitive scores, which are still not as good as **FLARE**, while KD and Reckoner fluctuate notably across datasets, and GoG tends to underperform, indicating weaker adaptability. These results confirm that **FLARE** sustains reliable predictive strength across domains of varying complexity and data heterogeneity.

**Table 1** extends this analysis to the subgroup level, revealing that **FLARE** maintains superior *beneficence* across known sensitive demographic partitions. In the OhioT1DM dataset, **FLARE** achieves significant improvements for *Pump* (**73.62%**) and *Age* (**74.36%**), outperforming ARL and KD by 5–10 percentage points. In the high-performing EDA dataset, where most models already approach saturation, **FLARE** still attains the best subgroup-wise scores (**89.1–89.5%**), confirming its robustness under low-variance conditions. Within the IHS dataset, which exhibits greater heterogeneity, **FLARE** achieves the highest F1-scores across all subgroups, ranging from **63.3% to 63.4%**. In comparison, ARL spans **62.5% to 62.7%**, while KD lags further behind at **58.0%–58.1%**.

This evaluation demonstrates that **FLARE** achieves stable and superior performance, both overall and across diverse subgroups, due to its architectural and training design. As discussed in Section 4.1, it employs an encoder–decoder architecture that captures temporal and contextual dependencies, combined with a Fisher-based penalty that stabilizes parameter updates during training—enhancing generalizability to unseen individuals and settings, measured through person-disjoint evaluations, while maintaining predictive reliability where other approaches often degrade. Moreover, the extended cluster adaptation and aggregation framework (Section 4.3) further improves efficacy by learning latent subgroup-specific rules, thereby promoting *beneficence*, while preserving stability, fairness, and preventing degradation.

Table 1. F1 scores (%) across demographic subgroups for different models in the OhioT1DM, EDA, and IHS datasets.

Subgroup	Benign Baseline (%)	KD (%)	ARL (%)	Reckoner (%)	GOG (%)	FLARE (%)
<b>OhioT1DM Dataset</b>						
Age	59.23	65.01	70.16	66.42	59.12	<b>74.36</b>
Cohort	63.31	67.33	70.46	67.57	63.50	<b>72.91</b>
Sex	64.79	68.08	70.71	68.51	65.09	<b>72.72</b>
Pump	53.59	60.66	65.80	61.74	53.92	<b>73.62</b>
Sensor Band	63.31	67.33	70.46	67.57	63.50	<b>72.91</b>
<b>EDA Dataset</b>						
Group_label	86.91	69.20	87.61	85.55	87.03	<b>89.08</b>
Sex	86.92	69.20	87.61	85.84	87.04	<b>89.47</b>
<b>IHS Dataset</b>						
Sex	59.66	58.12	62.69	57.52	59.93	<b>63.40</b>
Age	57.37	57.90	62.54	53.34	54.83	<b>63.29</b>
Ethnicity	56.37	58.06	62.66	52.85	57.67	<b>63.30</b>
Specialty	60.27	58.01	62.62	56.94	60.56	<b>63.30</b>
PHQ10>0	62.52	58.09	62.68	58.85	59.35	<b>63.37</b>

A more detailed subgroupwise analysis is shown in Appendix A.3.

**6.2.2 BHE Comparison of FLARE with SoTA FWD Baselines.** Comparing SoTA FWD approaches with **FLARE** through the lens of **benefit** (*B*), **harm avoidance** (*H*), and **equity** (*E*)—collectively the **BHE** dimensions—is essential to evaluate not only predictive accuracy but also ethical reliability. Improvements in one dimension

Table 2. Model-wise percentage changes ( $\Delta B$ ,  $\Delta H$ ,  $\Delta E$ ) for ARL, KD, Reckoner, GoG, and **FLARE** across datasets. Values represent percentage-point improvements, where larger deltas indicate stronger fairness performance and greater ethical consistency across subgroups.

Subgroup	ARL (%)			KD (%)			Reckoner (%)			GoG (%)			FLARE (%)		
	$\Delta B$	$\Delta H$	$\Delta E$	$\Delta B$	$\Delta H$	$\Delta E$	$\Delta B$	$\Delta H$	$\Delta E$	$\Delta B$	$\Delta H$	$\Delta E$	$\Delta B$	$\Delta H$	$\Delta E$
<b>OhioT1DM Dataset</b>															
Age	10.93%	3.98%	6.55%	5.78%	2.53%	4.82%	7.19%	2.08%	5.05%	-0.11%	-1.26%	0.52%	15.14%	5.35%	15.37%
Cohort	7.15%	2.32%	6.83%	4.01%	1.39%	-17.27%	4.26%	0.53%	3.90%	0.19%	-0.22%	-0.58%	9.60%	2.64%	9.83%
Sex	5.92%	2.46%	4.89%	3.29%	1.47%	2.58%	3.72%	2.98%	1.57%	0.30%	0.18%	-0.18%	7.93%	2.89%	3.04%
Pump	12.20%	4.86%	10.38%	7.07%	2.66%	6.23%	8.15%	2.92%	7.75%	0.32%	0.24%	0.12%	20.03%	5.41%	19.41%
Sensor Band	7.15%	2.32%	6.83%	4.01%	1.39%	3.72%	4.26%	0.53%	3.90%	0.19%	-0.22%	-0.58%	9.60%	2.64%	9.83%
<i>mean</i>	8.67%	3.19%	7.09%	4.83%	1.89%	0.01%	5.52%	1.81%	4.43%	0.18%	-0.26%	-0.14%	<b>12.46%</b>	<b>3.79%</b>	<b>11.50%</b>
<b>EDA Dataset</b>															
Group_label	0.70%	-0.42%	1.13%	-17.72%	-13.86%	2.06%	-1.37%	-23.22%	-2.36%	0.12%	-1.95%	-0.11%	2.16%	0.70%	0.57%
Sex	0.69%	-0.48%	-1.48%	-17.72%	-12.93%	-0.17%	-1.08%	-34.15%	2.30%	0.12%	-1.63%	0.22%	2.55%	0.68%	0.06%
<i>mean</i>	0.69%	-0.45%	-0.18%	-17.72%	-13.39%	<b>0.94%</b>	-1.22%	-28.69%	-0.03%	0.12%	-1.79%	0.06%	<b>2.36%</b>	<b>0.69%</b>	0.31%
<b>IHS Dataset</b>															
Sex	3.03%	2.28%	-0.73%	-1.54%	-2.81%	-1.40%	-2.14%	-2.84%	-1.51%	0.27%	-1.18%	-1.79%	3.74%	2.72%	0.04%
Age	5.18%	0.28%	-27.07%	0.54%	-22.67%	1.95%	-4.03%	-14.04%	5.03%	-2.54%	-31.82%	3.71%	5.92%	0.00%	8.95%
Ethnicity	6.29%	1.84%	-1.21%	1.69%	-9.20%	1.81%	-3.52%	-4.21%	-0.86%	1.30%	-3.08%	-6.76%	6.94%	0.00%	2.08%
Specialty	2.36%	0.00%	0.94%	-2.26%	-6.07%	0.59%	-3.32%	-7.69%	2.03%	0.29%	-2.95%	-0.25%	3.03%	0.68%	1.16%
PHQ10>0	0.15%	0.57%	1.88%	-4.43%	-4.90%	2.55%	-3.68%	-4.21%	2.34%	-3.17%	-7.34%	3.60%	0.85%	2.92%	3.25%
<i>mean</i>	3.40%	0.99%	-5.24%	-1.20%	-9.13%	1.10%	-2.06%	-3.03%	0.08%	0.62%	<b>4.12%</b>	0.09%	<b>4.09%</b>	1.26%	<b>3.09%</b>

at the expense of another lead to ethical inconsistencies, yielding models that appear accurate overall yet still propagate subgroup harm or inequity. Therefore, BHE metric provides a principled measure of whether fairness interventions genuinely improve ethical alignment.

To assess this, we evaluated three datasets—OhioT1DM, IHS, and EDA—reporting percentage-point changes ( $\Delta B$ ,  $\Delta H$ ,  $\Delta E$ ) relative to the Benign Baseline (Table 2). Across datasets, **FLARE** achieves the most coherent improvements across all BHE dimensions. On the OhioT1DM dataset, it records the highest mean deltas (**+12.46**, **+3.79**, **+11.50**), outperforming ARL (**+8.67**, **+3.19**, **+7.09**) and Reckoner (**+5.52**, **+1.81**, **+4.43**), while KD (**+4.83**, **+1.89**, **+0.01**) and GoG (**+0.18**, **-0.26**, **-0.14**) show minimal or unstable gains. Subgroup-level analysis reveals particularly strong improvements for *Pump* (**+20.03**, **+5.41**, **+19.41**) and *Age* (**+15.14**, **+5.35**, **+15.37**), demonstrating **FLARE**'s ability to correct high-variance bias sources without overcompensation. In the IHS dataset, which is more heterogeneous, **FLARE** sustains robust mean improvements (**+4.09**, **+1.26**, **+3.09**) while other FWD baselines regress in at least one dimension. Similarly, in the fairness-saturated EDA dataset, it continues to achieve balanced positive deltas (**+2.36**, **+0.69**, **+0.31**), whereas ARL and KD both exhibit degradation.

These results indicate that **FLARE** is uniquely capable of maintaining stability while improving fairness across multiple ethical axes, unlike adversarial or distillation-based approaches that tend to oscillate or overcorrect under imbalance. The reasons for this robustness align with **FLARE**'s theoretical design. Existing SoTA FWD methods enforce fairness globally—through uniform reweighting or adversarial gradients—without accounting for local heterogeneity in data geometry. In contrast, **FLARE** operates locally by identifying clusters of samples with similar geometric and model behavioral properties. Fisher penalty guides this process by capturing curvature-driven sensitivity, revealing which samples lie in unstable regions of the loss landscape. The cluster adaptation mechanism then fine-tunes these regions individually, while conditional aggregation transfers knowledge only when it demonstrably improves validation performance, avoiding the destructive averaging common in global aggregation. This balance between *local specialization* and *controlled sharing* explains why **FLARE** achieves both higher fairness and more stable optimization, as reflected by its consistently superior BHE scores across datasets.

**6.2.3 Empirical Validation of Attaining Autonomy at the User Level.** *Autonomy* requires AI systems to deliver consistent and stable behavior [19, 38, 65]. In this section, we extend the concept of autonomy to the user level, examining whether **FLARE** maintains stable and reliable performance across individual users. Real-world human-sensing data often exhibit substantial heterogeneity in physiology, behavior, context, and device use—factors that commonly lead to uneven performance across individuals [24, 90]. By evaluating user-level consistency, we assess **FLARE**'s ability to mitigate inter-user variability and sustain uniform accuracy and stability.

To this end, Fig. 3 compares six representative models—Benign Baseline, KD, ARL, Reckoner, GOG, and **FLARE**—across three datasets (OhioT1DM, EDA, and IHS). Each subplot reports the user-level *F1 mean* and *F1 standard deviation (F1 std)*, representing predictive accuracy and consistency, respectively. Including the Benign Baseline enables us to assess whether advanced fairness-oriented methods and **FLARE** improve upon a simple, unregularized model both in accuracy and reliability—key aspects of practical *autonomy*.

Across all datasets, **FLARE** demonstrates superior predictive performance while maintaining the lowest or among the lowest F1 variability across users:

- On **OhioT1DM**, **FLARE** achieves the highest F1 mean of **73.32%**, outperforming the Benign Baseline (**61.80%**), KD (66.63%), and ARL (69.56%), while reducing F1 std to **7.38%** compared to 12–18% for the baselines.
- On **EDA**, **FLARE** attains **88.86%** mean F1 with an F1 std of only **11.09%**, improving upon the Benign Baseline (**86.92%**, **13.39%**) and surpassing other fairness-oriented models such as ARL (87.67%, 11.38%) and GOG (87.06%, 13.67%).
- On **IHS**, **FLARE** achieves **62.57%** mean F1, outperforming the Benign Baseline (**57.41%**), KD (56.92%), and Reckoner (55.43%), with a comparable F1 std of **14.60%**.

These results indicate that **FLARE**'s *autonomy* enhancement extends to the user level, addressing the inherent human heterogeneity.

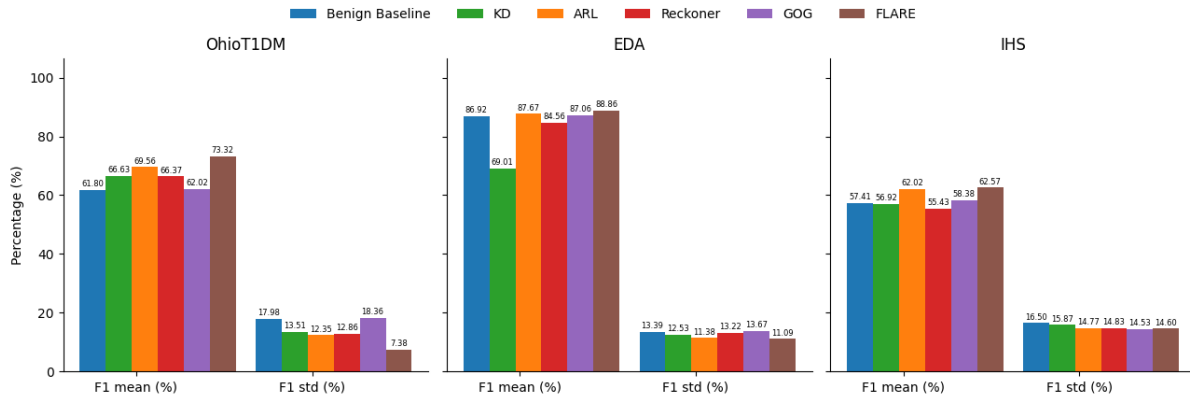


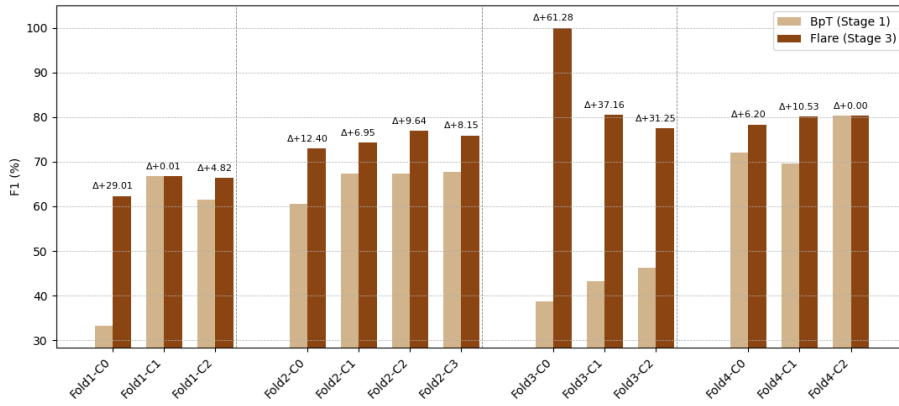
Fig. 3. User-level F1 mean and F1 standard deviation across all models for the OhioT1DM, EDA, and IHS datasets. Lower F1 std indicates more consistent model behavior, supporting user-level *autonomy*.

**6.2.4 Empirical Validation of the “Do Not Harm” Strategy.** This section serves as an internal *non-maleficence* validation of the **FLARE** framework, confirming that the adaptive clustering and aggregation mechanisms behave as intended—enhancing local specialization while ensuring that no cluster experiences a reduction in predictive performance compared to the pretrained classifier. It analyzes the change in F1-scores between the intermediate

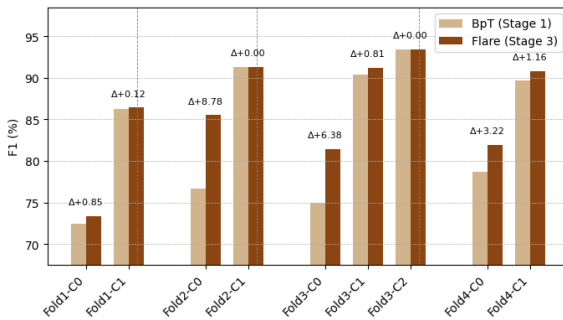
‘Base Pretrained (*BpT*)’ classifier (Section 4.1), and the final **FLARE** model for every dataset, fold, and cluster (Figure 4).

Across all datasets, the observed  $\Delta F1$  values are non-negative, indicating that **FLARE** consistently maintains or improves performance relative to the intermediate *BpT* stage. This stability verifies that the adaptive training dynamics of **FLARE** adhere to the *Do Not Harm* principle: the final model strengthens fairness and representation quality without introducing any degradation across clusters, folds, or subgroups.

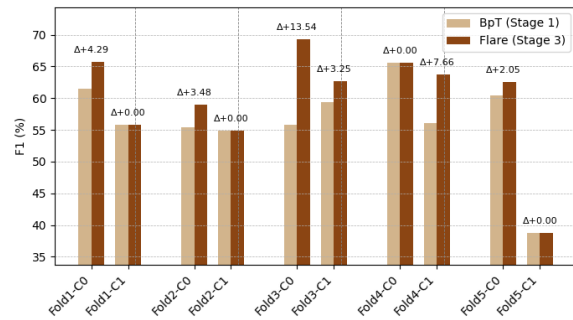
In the OhioT1DM dataset, several clusters show pronounced gains (e.g., Fold 3—Cluster 1: +44.65%, Cluster 2: +38.81%), indicating that the final-stage adaptation enhances generalization without sacrificing performance. For EDA, improvements are moderate yet consistent, demonstrating that even in already high-performing conditions, **FLARE** refines decision boundaries and sustains comparable or improved accuracy (e.g., Fold 2—Cluster 0: +8.81%, Fold 3—Cluster 0: +7.73%). In the more heterogeneous IHS dataset, stable positive shifts (e.g., Fold 3—Cluster 0: +17.14%) further demonstrate that the cluster-level adaptation sustains or improves accuracy within clusters, validating the do-no-harm objective.



(a) OhioT1DM: BpT vs. **FLARE** per fold-cluster.



(b) EDA: BpT vs. **FLARE** per fold-cluster.



(c) IHS: BpT vs. **FLARE** per fold-cluster.

Fig. 4. Fold and Cluster-wise F1 comparison across datasets within the proposed **FLARE** framework. Bars show F1-scores for Base preTraining (BpT, light brown) as the intermediate module (1) and **FLARE** (dark brown) as the final module (3) across all fold-cluster pairs. Values above each pair ( $\Delta$ ) indicate the change from BpT to **FLARE**.

### 6.3 Validating Design Choices

We validate **FLARE**'s design choices through two complementary analyses, ensuring that its observed improvements directly result from the intended design principles. First, we visualize and compare the *loss landscapes* of models trained with and without Fisher penalty regularization to examine how curvature control influences optimization stability and generalization. Second, we perform a detailed *component-level ablation* of the network structure to isolate the contribution of Fisher regularization, cluster adaptation, and conditional aggregation. Together, these analyses clarify why **FLARE** converges to flatter, more stable minima and how each architectural element contributes to improved ethical fairness.

**6.3.1 Analyzing Optimization Geometry through Loss Landscapes.** To substantiate the design choices underpinning **FLARE** and to interpret its behavior from an optimization–geometry perspective, we visualize the loss landscapes [54] corresponding to the best-performing **FLARE** models across all three datasets—OhioT1DM, EDA, and IHS. Specifically, we examine how each design component (base pretraining, Fisher penalty regularization, and cluster-level adaptation with do-no-harm aggregation) shapes the curvature and smoothness of the resulting optimization surface.

Prior research has established that the geometry of the loss landscape encodes valuable generalization properties: models converging to flatter minima exhibit better generalization performance [52, 54, 73]. In contrast, sharper minima indicate higher curvature regions that correspond to overfitting and unstable learning dynamics. Following [54], we visualize the loss by sweeping along two random, filter-normalized orthogonal directions (denoted as  $X$ - and  $Y$ -steps), with the  $Z$ -axis representing the corresponding loss surface centered at the final converged weights.

Figure 5 illustrates the comparative loss landscapes for four ablated variants—(i) the benign baseline model, (ii) base pretraining without the Fisher penalty (*BpT-wo Fisher*), (iii) base pretraining with Fisher penalty regularization (*BpT-w Fisher*), and (iv) **FLARE** (*BpT-w Fisher + Adaptation*). These are shown separately for the EDA (Figure 5a), IHS (Figure 5b), and OhioT1DM datasets (Figure 5c), each generated using identical folds and cluster data for fair, unbiased comparison.

Across all datasets, we consistently observe that the benign baseline exhibits a turbulent and sharp loss surface (highlighted with red arrows and dotted circles), characterized by *steep valleys and narrow basins*. Such sharp curvature regions imply *higher local sensitivity to parameter perturbations and are indicative of overfitting* [52].

Introducing the base pretraining step without Fisher penalty regularization (second subfigure, red arrows) results in a visibly smoother surface, but it still retains local irregularities. Incorporating the Fisher penalty (orange arrows and dotted circles) further stabilizes the curvature, reducing sharpness and yielding a broader, lower-energy basin that captures the effect of curvature-aware regularization [20].

The full **FLARE** model (rightmost panels, highlighted with green arrows and dotted circles) demonstrates a consistently flatter and wider basin across all datasets, representing a near-flat optimum. This outcome reflects the synergistic effect of cluster-specific adaptation and stability-preserving aggregation—where the do-no-harm regularizer ensures local fine-tuning benefits subgroups without regressing from the baseline. The flatter landscape empirically supports our claim of **FLARE** achieving a Pareto-optimal [67], i.e., "Do not harm" balance between performance improvement and fairness preservation.

These results suggest that **FLARE**, effectively steers the optimization towards smoother and more generalizable minima by penalizing curvature (via Fisher penalty) and harmonizing subgroup-specific fine-tuning through adaptive aggregation. The observed flattening across datasets provides geometric evidence that our design enhances both robustness and fairness, aligning with the intended Pareto-optimal learning objectives.

**6.3.2 Assessing Structural Contributions via Detailed Ablation.** We conducted an ablation study to assess the contribution of each structural component within **FLARE**, specifically examining the individual and combined effects of Fisher penalty regularization and the Cluster Adaptation and Aggregation (CAA)

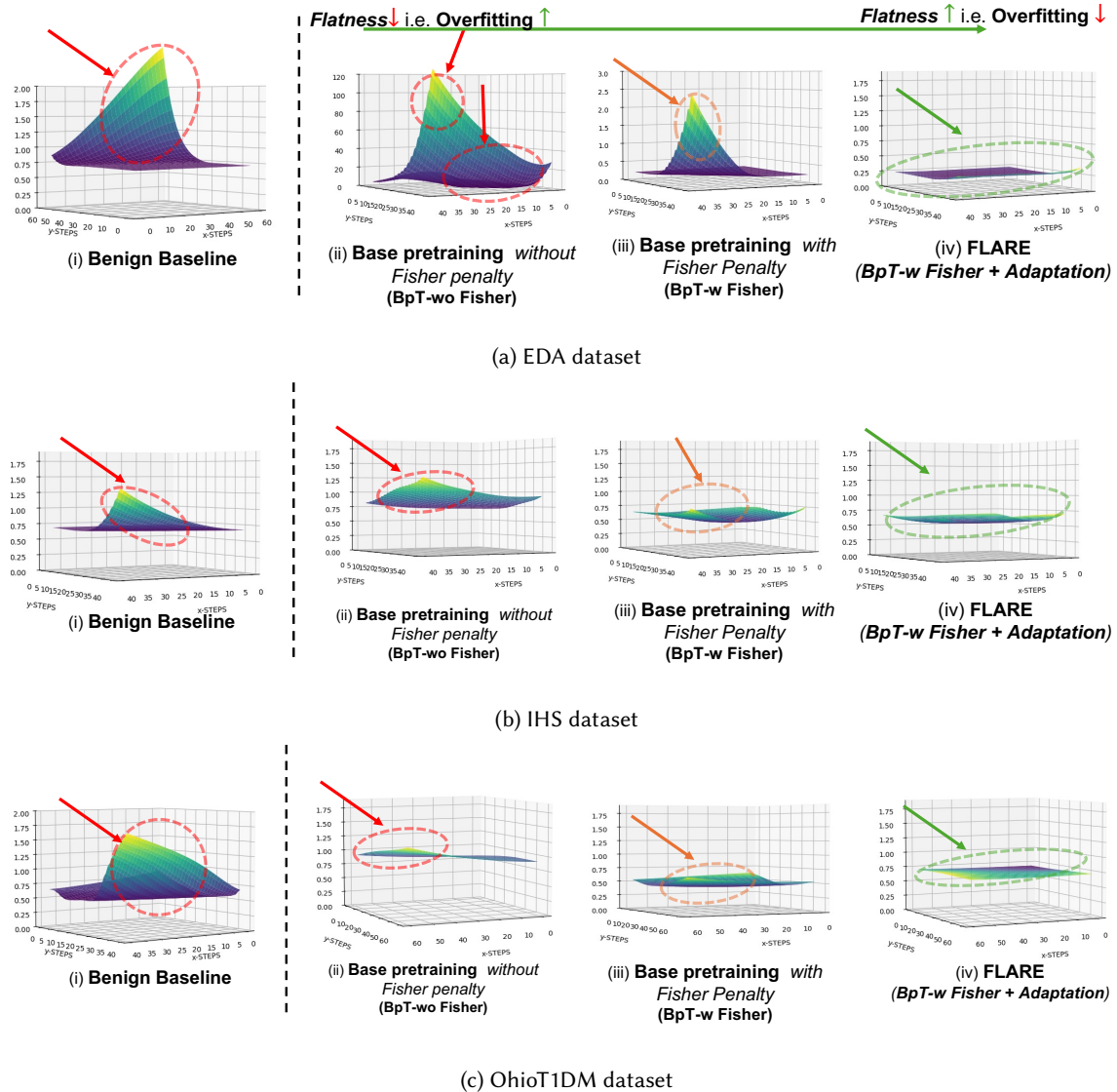


Fig. 5. Loss landscape visualizations for the benign baseline, base Pre-training without Fisher penalty, base pretraining with Fisher penalty regularization, and **FLARE** across three datasets. The *red*, *orange*, and *green* arrows and dotted circles respectively highlight curvature transitions, showing how Fisher regularization and cluster adaptation progressively flatten the optimization landscape.

module. This analysis disentangles how each element influences fairness, stability, and overall performance across datasets. Table 3 summarizes the results, demonstrating that Fisher penalty regularization enhances representational smoothness and equity, while CAA enhances performance, while avoiding harm across latent clusters. The full **FLARE** configuration—combining both components—consistently achieves the most balanced and consistent improvements, confirming their complementary roles in achieving ethical fairness without demographic supervision.

We compare four configurations:

- **BpT-w Fisher**, base pretraining with Fisher penalty regularization;
- **BpT-wo Fisher**, the same base pretraining procedure without Fisher penalty;
- **CAA-wo Fisher**, which uses the same Cluster Adaptation and Aggregation (CAA) module as **FLARE**, but initializes from a non-Fisher penalty base; and
- the full **FLARE** model, combining both.

Across all datasets, Fisher penalty regularization during base pretraining improves representational stability and equity. In the OhioT1DM dataset, BpT-w Fisher produces modest gains ( $\Delta B = +0.74$ ,  $\Delta H = -2.13$ ,  $\Delta E = -1.27$ ), while removing Fisher (BpT-wo Fisher) increases *beneficence* (+7.96) but with fluctuating harm and equity (+0.80, +9.05), indicating less controlled adaptation. Introducing the CAA module without Fisher further raises  $\Delta E$  (+5.62) but amplifies harm variability ( $\Delta H = -9.53$ ), highlighting its sensitivity to unstable initialization. When both components are integrated, **FLARE** achieves the strongest and most consistent improvements (+12.46, +3.79, +11.50), demonstrating that Fisher penalty regularization and CAA work synergistically—one stabilizing the base representation and the other refining subgroup alignment.

In the EDA dataset, all configurations improve slightly, but **FLARE** attains the highest overall balance (+2.36, +0.69, +0.31), whereas BpT-w Fisher (+1.49, -0.32, +1.22) and BpT-wo Fisher (+1.91, -0.51, +1.08) show smaller or inconsistent changes. This pattern reinforces that the Fisher penalty-informed base provides a smoother optimization surface for subsequent cluster adaptation.

The IHS dataset, characterized by high heterogeneity, further confirms this trend. BpT-w Fisher achieves minor positive *beneficence* (+0.65) but negative harm and equity values, while BpT-wo Fisher and CAA-wo Fisher exhibit larger oscillations in  $\Delta H$  (-4.90 and -5.10 respectively). Only **FLARE** yields consistent positive deltas across all three dimensions (+4.09, +6.00, +3.09), indicating stable adaptation under complex population shifts.

These findings collectively demonstrate that Fisher regularization establishes a stable and equitable representational foundation, while the Cluster Adaptation and Aggregation (CAA) module leverages this stability to refine subgroup alignment and performance.

## 7 On-device Efficiency during Wearable Model Inference

Evaluating on-device inference efficiency is critical for human sensing systems, particularly those that rely on resource-constrained wearables such as the Empatica E4 used in our *EDA* dataset. In such systems, inference latency and memory consumption directly determine the feasibility of real-time feedback and energy sustainability [50, 79]. Therefore, to evaluate the practical feasibility of **FLARE** during deployment, we benchmarked its on-device inference efficiency against the baselines (Benign, ARL, KD, Reckoner, GoG) across five hardware platforms—from high-end GPUs (NVIDIA RTX 4090, Quadro RTX 5000) to desktop-class CPUs (Intel i9-9900K, AMD Ryzen 9 7950X, Apple M1) for the *EDA* dataset. We measured the average inference time, resident set size (RSS) memory usage, and resource utilization percentage (CPU/GPU utilization) over five runs per platform. Table 4 presents the results for the *EDA* dataset. **FLARE** maintains similar inference latency and memory consumption across all devices with consistently low latency—0.001 s on the RTX 4090, 0.006 s on the Ryzen 9, and 0.04 s on the Apple M1 while consuming modest memory (~ 826 Mbs on average). Resource utilization remains minimal ( $\leq 4\%$  GPU and  $\leq 3.5\%$  CPU), demonstrating efficient hardware usage even on edge devices. The low CPU utilization reflects measurements normalized across all available cores on multi-core processors, where lightweight inference workloads engage only a subset of threads, an expected behavior in energy-efficient human-sensing models [32, 40]. Notably, **FLARE**, with its two-stage learning process, learns cluster memberships once during the base-pretraining phase and only uses them during inference, thus ensuring efficient inference time performance without compromising deployability on heterogeneous systems.

Table 3. Ablation study showing percentage changes ( $\Delta B$ ,  $\Delta H$ ,  $\Delta E$ ) for Base-Training with Fisher (BpT-w Fisher), Base-Training without Fisher (BpT-wo Fisher), Cluster Adaptation and Aggregation without base-trained Fisher (CAA-wo Fisher), and **FLARE** across datasets. Values are percentage points.

Subgroup	BpT-w Fisher (%)			BpT-wo Fisher (%)			CAA-wo Fisher (%)			FLARE (%)		
	$\Delta B$	$\Delta H$	$\Delta E$	$\Delta B$	$\Delta H$	$\Delta E$	$\Delta B$	$\Delta H$	$\Delta E$	$\Delta B$	$\Delta H$	$\Delta E$
<b>OhioT1DM Dataset</b>												
Age	2.21%	-2.26%	0.68%	10.23%	2.29%	12.65%	5.61%	-7.75%	9.69%	15.14%	5.35%	15.37%
Cohort	0.16%	-2.72%	-16.92%	5.78%	-0.08%	8.29%	1.52%	-11.25%	2.92%	9.60%	2.64%	9.83%
Sex	-0.39%	-2.10%	2.41%	4.13%	-0.54%	-0.21%	-2.02%	-9.13%	0.11%	7.93%	2.89%	3.04%
Pump	1.56%	-0.85%	3.40%	13.90%	2.41%	16.25%	11.24%	-8.29%	12.47%	20.03%	5.41%	19.41%
Sensor Band	0.16%	-2.72%	4.07%	5.78%	-0.08%	8.29%	1.52%	-11.25%	2.92%	9.60%	2.64%	9.83%
<i>mean</i>	0.74%	-2.13%	-1.27%	7.96%	0.80%	9.05%	3.58%	-9.53%	5.62%	<b>12.46%</b>	<b>3.79%</b>	<b>11.50%</b>
<b>EDA Dataset</b>												
Group_label	1.50%	-0.51%	2.13%	1.98%	0.03%	0.96%	1.97%	0.11%	2.13%	2.16%	0.70%	0.57%
Sex	1.49%	-0.13%	0.31%	1.83%	-1.06%	1.19%	1.97%	0.46%	0.47%	2.55%	0.68%	0.06%
<i>mean</i>	1.49%	-0.32%	1.22%	1.91%	-0.51%	1.08%	1.97%	0.28%	1.30%	<b>2.36%</b>	<b>0.69%</b>	<b>0.31%</b>
<b>IHS Dataset</b>												
Sex	0.07%	-0.33%	-0.57%	0.92%	0.48%	-0.37%	0.65%	0.03%	-0.36%	3.74%	2.90%	0.04%
Age	3.78%	-3.14%	1.39%	2.45%	-9.77%	2.20%	2.83%	-9.77%	7.94%	5.92%	12.42%	8.95%
Ethnicity	0.29%	-2.23%	-2.74%	-0.85%	-2.11%	-9.45%	-0.06%	-2.27%	2.38%	6.94%	5.22%	2.08%
Specialty	-0.06%	-2.75%	-0.35%	0.68%	-7.25%	0.94%	3.78%	-7.37%	1.07%	3.03%	5.66%	1.16%
PHQ10>0	-0.82%	-1.81%	1.40%	1.62%	-5.85%	-1.07%	-2.22%	-6.09%	2.89%	0.85%	3.79%	3.25%
<i>mean</i>	0.65%	-2.05%	-0.17%	0.96%	-4.90%	-1.55%	0.99%	-5.10%	2.78%	<b>4.09%</b>	<b>6.00%</b>	<b>3.09%</b>

Table 4. Inference Time (s), Inference Process (RSS) Memory Usage (MB), and Inference Resource Usage (%) for baselines and **FLARE** across different platforms evaluated for the EDA dataset.

Platform	Benign Baseline			ARL			KD			Reckoner			GoG			FLARE		
	Infer (s)	RSS (MB)	Usage (%)	Infer (s)	RSS (MB)	Usage (%)	Infer (s)	RSS (MB)	Usage (%)	Infer (s)	RSS (MB)	Usage (%)	Infer (s)	RSS (MB)	Usage (%)	Infer (s)	RSS (MB)	Usage (%)
<b>EDA Dataset</b>																		
NVIDIA GeForce RTX 4090	0.001	1214.7	21	0.006	1256.6	26	0.077	1269.3	28	0.01	1288	13.8	0.01	1625	18.4	0.001	1070	4
AMD Ryzen 9 7950X 16-Core Processor	0.01	1219.6	0.78	0.006	1263	0.79	0.005	1274.7	0.82	0.01	1351.7	0.78	0.01	1648	1.09	0.006	1073	1.13
Quadro RTX 5000	0.12	983.7	7.90	0.02	1020.1	11.7	0.02	1031.3	10.90	0.05	1146.4	5.0	0.03	1414.1	34.8	0.02	818.8	2.40
Intel i9-9900K Processor	0.07	1133.4	3.11	0.08	1129	3.12	0.0541	1143	3.12	0.27	1234.7	3.01	0.09	1515.8	3.68	0.02	840.1	3.12
Apple M1	0.02	133.3	0.72	0.017	157.0	0.65	0.01	135.8	0.59	0.03	98.1	0.25	0.02	173.4	0.74	0.04	331.9	0.20

## 8 Discussions and Limitations

While **FLARE** advances ethical, demographic-agnostic fairness, it also presents computational and methodological considerations that open avenues for future research and refinement.

- (1) **Training-Time Overhead and Practical Feasibility.** While **FLARE**'s inference-time performance matches SoTA baselines (refer to Section 7), our approach incurs additional training-time overhead due to the base

pre-training phase for latent subgroup identification and clustering. Our Train time evaluation in Appendix A.4 shows that for the EDA dataset, although the training latency is higher, the CPU and memory utilization remain comparable to other approaches. In practice, this overhead is manageable since most human-sensing systems rely on centralized or edge/cloud-based training pipelines capable of handling increased computational demands [7, 47, 63, 66]. Hence, FLARE’s added training cost is a reasonable trade-off for its fairness and ethical consideration gains, especially since deployment emphasizes lightweight inference rather than on-device training.

- (2) **Influence of Person-Disjoint Splits on Reported Accuracy.** Notably, our results on the **OhioT1DM** dataset show lower accuracy than those reported in prior work [61]; this difference stems from this paper’s stricter and more realistic evaluation protocol. Unlike previous studies that used overlapping user data, our *person-disjoint evaluation* ensures complete subject-level separation between the training and testing sets. This setup prevents information leakage and provides a more faithful estimate of real-world generalization to unseen individuals, reflecting robustness rather than overfitting to user-specific patterns.
- (3) **Interpretability of Latent Subgroups.** FLARE identifies latent subgroups through clustering based on model embeddings and instance-level loss and landscape curvature, without relying on explicit demographic or sensitive attributes. However, this optimization-driven process makes it difficult to determine which demographic or sensitive factors—or their combinations—underlie the observed disparities. As noted in Section 3.2, we assess ethical fairness using known demographic attributes only as proxies for unobserved ones. This limitation is not unique to our framework; existing fairness-without-demographics (FWD) approaches [14, 49, 59, 68] face the same challenge. Nevertheless, identifying the hidden social or contextual factors behind such latent disparities remains a valuable direction for future research, as doing so could inform more transparent, data-aware, and socially responsible AI interventions.
- (4) **Experiment at Scale.** Due to the scarcity of large, demographically annotated human-sensing datasets, our evaluation could not be conducted on broader-scale cohorts. While our experiments spanned diverse domains—wearable sensing (EDA), mobile sensing in the wild (IHS), and clinical monitoring (OhioT1DM)—datasets encompassing multiple sensitive attributes remain rare in the human-sensing domain [94]. Even recent large-scale initiatives such as GLOBEM [92] omit demographic or sensitive information due to privacy, consent, and ethical constraints [56], a gap also noted across ubiquitous and mobile sensing research [93, 95]. Developing ethically curated datasets that balance participant privacy with the inclusion of demographic or sensitive information will be essential for future large-scale validation of FLARE and broader fairness research in human-centered AI.

## 9 Conclusion

This paper introduced FLARE—the first principled framework for achieving ethical fairness without access to demographic information. It provides a demographic-agnostic and ethically grounded foundation for human-centered AI, detecting and mitigating latent disparities through geometry-aware collaboration rather than demographic supervision. Comprehensive evaluations across diverse human-centered datasets and its computational efficiency on edge devices demonstrate FLARE’s practicality for real-world, resource-constrained deployment. As AI systems increasingly influence critical decisions that shape human welfare, embedding fairness and ethics into their core design is essential for building systems that are trustworthy, inclusive, and accountable. FLARE represents a step toward this future—realizing practical, ethically aligned AI with transformative implications for sensitive and high-impact domains such as healthcare, education, and behavioral sensing.

## References

- [1] ADLER, D. A., TSENG, V. W.-S., QI, G., SCARPA, J., SEN, S., AND CHOUDHURY, T. Identifying mobile sensing indicators of stress-resilience. *Proceedings of the ACM on Interactive, Mobile, Wearable and Ubiquitous Technologies* 5, 2 (2021), 1–32.

- [2] ADLER, D. A., YANG, Y., VIRANDA, T., XU, X., MOHR, D. C., VAN METER, A. R., TARTAGLIA, J. C., JACOBSON, N. C., WANG, F., ESTRIN, D., ET AL. Beyond detection: Towards actionable sensing research in clinical mental healthcare. *Proceedings of the ACM on interactive, mobile, wearable and ubiquitous technologies* 8, 4 (2024), 1–33.
- [3] AFROSE, S., SONG, W., NEMEROFF, C. B., LU, C., AND YAO, D. Subpopulation-specific machine learning prognosis for underrepresented patients with double prioritized bias correction. *Communications medicine* 2, 1 (2022), 111.
- [4] AI, N. Artificial intelligence risk management framework (ai rmf 1.0). URL: <https://nvlpubs.nist.gov/nistpubs/ai/nist.ai> (2023), 100–1.
- [5] AKANDE, O. A. Architecting decentralized ai frameworks for multi-modal health data fusion to advance equitable and personalized medicine.
- [6] ALABI, M. Ethical implications of ai: Bias, fairness, and transparency, 2024.
- [7] ALAWNEH, L., AL-AYYOUB, M., AL-SHARIF, Z. A., AND SHATNAWI, A. Personalized human activity recognition using deep learning and edge-cloud architecture. *Journal of Ambient Intelligence and Humanized Computing* 14, 9 (2023), 12021–12033.
- [8] ANDERSSON, G. B., CHAPMAN, J. R., DEKUTOSKI, M. B., DETTORI, J., FEHLINGS, M. G., FOURNEY, D. R., NORVELL, D., AND WEINSTEIN, J. N. Do no harm: the balance of “beneficence” and “non-maleficence”, 2010.
- [9] ANDRUS, M., AND VILLENEUVE, S. Demographic-reliant algorithmic fairness: Characterizing the risks of demographic data collection in the pursuit of fairness. In *Proceedings of the 2022 ACM Conference on Fairness, Accountability, and Transparency* (2022), pp. 1709–1721.
- [10] AREFEEN, A., AND GHASEMZADEH, H. Designing user-centric behavioral interventions to prevent dysglycemia with novel counterfactual explanations. *arXiv preprint arXiv:2310.01684* (2023).
- [11] ARIZE AI. Evaluating model fairness, May 2023. Responsible AI. Discusses bias and fairness in machine learning, including sensitive and non-sensitive group bias, and approaches to mitigate bias in model development.
- [12] BENZINGER, L., URSIN, F., BALKE, W.-T., KACPROWSKI, T., AND SALLOCH, S. Should artificial intelligence be used to support clinical ethical decision-making? a systematic review of reasons. *BMC medical ethics* 24, 1 (2023), 48.
- [13] BEUTEL, A., CHEN, J., DOSHI, T., QIAN, H., WOODRUFF, A., LUU, C., KREITMANN, P., BISCHOF, J., AND CHI, E. H. Putting fairness principles into practice: Challenges, metrics, and improvements. In *Proceedings of the 2019 AAAI/ACM Conference on AI, Ethics, and Society* (2019), pp. 453–459.
- [14] CHAI, J., JANG, T., AND WANG, X. Fairness without demographics through knowledge distillation. *Advances in Neural Information Processing Systems* 35 (2022), 19152–19164.
- [15] CHINTA, S. V., WANG, Z., YIN, Z., HOANG, N., GONZALEZ, M., QUY, T. L., AND ZHANG, W. Fairaid: Navigating fairness, bias, and ethics in educational ai applications. *arXiv preprint arXiv:2407.18745* (2024).
- [16] DADA, B. A., NWULU, N. I., AND OLUKANMI, S. O. Bayesian optimization with optuna for enhanced soil nutrient prediction: A comparative study with genetic algorithm and particle swarm optimization. *Smart Agricultural Technology* (2025), 101136.
- [17] DAUPHIN, Y. N., AGARWALA, A., AND MOBAHI, H. Neglected hessian component explains mysteries in sharpness regularization. *arXiv preprint arXiv:2401.10809* (2024).
- [18] EMMA, L. The ethical implications of artificial intelligence: A deep dive into bias, fairness, and transparency. Retrieved from Emma, L. (2024). *The Ethical Implications of Artificial Intelligence: A Deep Dive into Bias, Fairness, and Transparency* (2024).
- [19] FLORIDI, L., AND COWLS, J. A unified framework of five principles for ai in society. *Machine learning and the city: Applications in architecture and urban design* (2022), 535–545.
- [20] FORET, P., KLEINER, A., MOBAHI, H., AND NEYSHABUR, B. Sharpness-aware minimization for efficiently improving generalization. *arXiv preprint arXiv:2010.01412* (2021).
- [21] FRIEDLER, S. A., SCHEIDEGGER, C., AND VENKATASUBRAMANIAN, S. The (im) possibility of fairness: Different value systems require different mechanisms for fair decision making. *Communications of the ACM* 64, 4 (2021), 136–143.
- [22] FRIEDLER, S. A., SCHEIDEGGER, C., VENKATASUBRAMANIAN, S., CHOUDHARY, S., HAMILTON, E. P., AND ROTH, D. A comparative study of fairness-enhancing interventions in machine learning. In *Proceedings of the conference on fairness, accountability, and transparency* (2019), pp. 329–338.
- [23] GABRIEL, I. Toward a theory of justice for artificial intelligence. *Daedalus* 151, 2 (2022), 218–231.
- [24] GIBLON, R., GAO, C., LIU, K., OUYANG, Y., CUNNINGHAM, J., PIMIENTA, A., GOLIGHER, E., AND HEATH, A. Who benefits? uncovering hidden heterogeneity of treatment effects in adaptive trials using bayesian methods: A systematic review.
- [25] GIGUERE, S., METEVIER, B., BRUN, Y., DA SILVA, B. C., THOMAS, P. S., AND NIEKUM, S. Fairness guarantees under demographic shift. In *Proceedings of the 10th International Conference on Learning Representations (ICLR)* (2022).
- [26] GIOVANOLA, B., AND TIRIBELLI, S. Beyond bias and discrimination: redefining the ai ethics principle of fairness in healthcare machine-learning algorithms. *AI & society* 38, 2 (2023), 549–563.
- [27] GU, X., ZHANG, Z., JIN, R., GOH, R. S. M., AND LUO, T. Self-distillation with model averaging. *Information Sciences* 694 (2025), 121694.
- [28] HARDT, M., PRICE, E., AND SREBRO, N. Equality of opportunity in supervised learning. *Advances in neural information processing systems* 29 (2016).
- [29] HASHIMOTO, T., SRIVASTAVA, M., NAMKOONG, H., AND LIANG, P. Fairness without demographics in repeated loss minimization. In *International Conference on Machine Learning* (2018), PMLR, pp. 1929–1938.

- [30] HEALY, J., AND MCINNES, L. Uniform manifold approximation and projection. *Nature Reviews Methods Primers* 4, 1 (2024), 82.
- [31] HEBERT-JOHNSON, U., KIM, M., REINGOLD, O., AND ROTHBLUM, G. Multicalibration: Calibration for the (computationally-identifiable) masses. In *Proceedings of the 35th International Conference on Machine Learning (ICML)* (2018), pp. 1939–1948.
- [32] HIRSCH, M., MATEOS, C., AND MAJCHRZAK, T. A. Exploring smartphone-based edge ai inferences using real testbeds. *Sensors* 25, 9 (2025), 2875.
- [33] HOD, S., FILAN, D., CASPER, S., CRITCH, A., AND RUSSELL, S. Quantifying local specialization in deep neural networks. *arXiv preprint arXiv:2110.08058* (2021).
- [34] HOUSE, T. W. Removing barriers to american leadership in artificial intelligence. *Executive Order* 23 (2025).
- [35] HUANG, W., RONG, Y., XU, T., SUN, F., AND HUANG, J. Tackling over-smoothing for general graph convolutional networks. *arXiv preprint arXiv:2008.09864* (2020).
- [36] HURLEY, P. Fairness and beneficence. *Ethics* 113, 4 (2003), 841–864.
- [37] IZMAILOV, P., PODOPRIKHIN, D., GARIPPOV, T., VETROV, D., AND WILSON, A. G. Averaging weights leads to wider optima and better generalization. *arXiv preprint arXiv:1803.05407* (2018).
- [38] JAHN, W. T. The 4 basic ethical principles that apply to forensic activities are respect for autonomy, beneficence, nonmaleficence, and justice. *Journal of chiropractic medicine* 10, 3 (2011), 225.
- [39] JASTRZĘBSKI, S., KENTON, Z., BALLAS, N., FISCHER, A., BENGIO, Y., AND STORKEY, A. On the relation between the sharpest directions of dnn loss and the sgd step length. *arXiv preprint arXiv:1807.05031* (2018).
- [40] JIN, X., LI, L., DANG, F., CHEN, X., AND LIU, Y. A survey on edge computing for wearable technology. *Digital Signal Processing* 125 (2022), 103146.
- [41] JOBIN, A., IENCA, M., AND VAYENA, E. The global landscape of ai ethics guidelines. *Nature Machine Intelligence* 1, 9 (2019), 389–399.
- [42] KAMIRAN, F., AND CALDERS, T. Data preprocessing techniques for classification without discrimination. In *Knowledge and Information Systems* (2012), vol. 33, pp. 1–33.
- [43] KANG, S. K-nearest neighbor learning with graph neural networks. *Mathematics* 9, 8 (2021), 830.
- [44] KATIRAI, A. The ethics of advancing artificial intelligence in healthcare: analyzing ethical considerations for japan’s innovative ai hospital system. *Frontiers in Public Health* 11 (2023), 1142062.
- [45] KEARNS, M., NEEL, S., ROTH, A., AND WU, Z. S. Preventing fairness gerrymandering: Auditing and learning for subgroup fairness. In *Proceedings of the 35th International Conference on Machine Learning (ICML)* (2018), pp. 2564–2572.
- [46] KENFACK, P. J., KAHOU, S. E., AND AIVODJI, U. A survey on fairness without demographics. *Transactions on Machine Learning Research* (2024).
- [47] KHAN, A. R., MANZOOR, H. U., AYAZ, F., IMRAN, M. A., AND ZOHA, A. A privacy and energy-aware federated framework for human activity recognition. *Sensors* 23, 23 (2023), 9339.
- [48] KOH, P. W., SAGAWA, S., MARKLUND, H., XIE, S. M., ZHANG, M., BALSUBRAMANI, A., HU, W., YASUNAGA, M., PHILLIPS, R. L., GAO, I., ET AL. Wilds: A benchmark of in-the-wild distribution shifts. In *International conference on machine learning* (2021), PMLR, pp. 5637–5664.
- [49] LAHOTI, P., BEUTEL, A., CHEN, J., LEE, K., PROST, F., THAIN, N., WANG, X., AND CHI, E. Fairness without demographics through adversarially reweighted learning. *Advances in neural information processing systems* 33 (2020), 728–740.
- [50] LANE, N. D., AND GEORGIEV, P. Can deep learning revolutionize mobile sensing? In *Proceedings of the 16th international workshop on mobile computing systems and applications* (2015), pp. 117–122.
- [51] LEE, B.-K., KIM, J., AND RO, Y. M. Masking adversarial damage: Finding adversarial saliency for robust and sparse network. In *Proceedings of the IEEE/CVF Conference on Computer Vision and Pattern Recognition* (2022), pp. 15126–15136.
- [52] LI, A., ZHUANG, L., LONG, X., YAO, M., AND WANG, S. Seeking consistent flat minima for better domain generalization via refining loss landscapes. In *Proceedings of the Computer Vision and Pattern Recognition Conference* (2025), pp. 15349–15359.
- [53] LI, C., CAO, Z., AND LIU, Y. Deep ai enabled ubiquitous wireless sensing: A survey. *ACM Computing Surveys (CSUR)* 54, 2 (2021), 1–35.
- [54] LI, H., XU, Z., TAYLOR, G., STUDER, C., AND GOLDSTEIN, T. Visualizing the loss landscape of neural nets. *Advances in neural information processing systems* 31 (2018).
- [55] LI, Y., DANGEL, F., TAM, D., AND RAFFEL, C. Fishers for free? approximating the fisher information matrix by recycling the squared gradient accumulator. *arXiv preprint arXiv:2507.18807* (2025).
- [56] LINNA JR, D. W., AND MUCHMAN, W. J. Ethical obligations to protect client data when building artificial intelligence tools: Wigmore meets ai. *Prof. Law* 27 (2020), 27.
- [57] LIU, C. C., PFEIFFER, J., VULIĆ, I., AND GUREVYCH, I. Fun with fisher: Improving generalization of adapter-based cross-lingual transfer with scheduled unfreezing. *arXiv preprint arXiv:2301.05487* (2023).
- [58] LIU, E. Z., HAGHGOO, B., CHEN, A. S., RAGHUNATHAN, A., KOH, P. W., SAGAWA, S., LIANG, P., AND FINN, C. Just train twice: Improving group robustness without training group information. In *International Conference on Machine Learning* (2021), PMLR, pp. 6781–6792.
- [59] LUO, Y., LI, Z., LIU, Q., AND ZHU, J. Fairness without demographics through learning graph of gradients. In *Proceedings of the 31st ACM SIGKDD Conference on Knowledge Discovery and Data Mining V. 1* (2025), pp. 918–926.
- [60] MANJUNATH, N., LI, Z. Y., CHOI, E. S., SEN, S., WANG, F., AND ADLER, D. A. Can data augmentation improve daily mood prediction from

- wearable data? an empirical study. In *Adjunct Proceedings of the 2023 ACM International Joint Conference on Pervasive and Ubiquitous Computing & the 2023 ACM International Symposium on Wearable Computing* (2023), pp. 632–637.
- [61] MARLING, C., AND BUNESCU, R. The ohio1dm dataset for blood glucose level prediction: Update 2020. In *CEUR workshop proceedings* (2020), vol. 2675, p. 71.
- [62] MARTENS, J. New insights and perspectives on the natural gradient method. *Journal of Machine Learning Research* 21, 146 (2020), 1–76.
- [63] MESSER, A., GREENBERG, I., BERNADAT, P., MILOJICIC, D., CHEN, D., GIULI, T. J., AND GU, X. Towards a distributed platform for resource-constrained devices. In *Proceedings 22nd International Conference on Distributed Computing Systems* (2002), IEEE, pp. 43–51.
- [64] MISHLER, A., KENNEDY, E. H., AND CHOULDECHOVA, A. Fairness in risk assessment instruments: Post-processing to achieve counterfactual equalized odds. In *Proceedings of the 2021 ACM conference on fairness, accountability, and transparency* (2021), pp. 386–400.
- [65] MITTELSTADT, B. Principles alone cannot guarantee ethical ai. *Nature machine intelligence* 1, 11 (2019), 501–507.
- [66] MOSHAWRAB, M., ADDA, M., BOUZOUANE, A., IBRAHIM, H., AND RAAD, A. Reviewing federated machine learning and its use in diseases prediction. *Sensors* 23, 4 (2023), 2112.
- [67] NAGPAL, R., SHAHSAVARIFAR, R., GOYAL, V., AND GUPTA, A. Optimizing fairness and accuracy: a pareto optimal approach for decision-making. *AI and Ethics* 5, 2 (2025), 1743–1756.
- [68] NI, H., HAN, L., CHEN, T., SADIQ, S., AND DEMARTINI, G. Fairness without sensitive attributes via knowledge sharing. In *Proceedings of the 2024 ACM Conference on Fairness, Accountability, and Transparency* (2024), pp. 1897–1906.
- [69] OPOKU, R. A., PEI, B., AND XING, W. Unveiling accuracy-fairness trade-offs: Investigating machine learning models in student performance prediction. *Journal of Learning Analytics* 12, 2 (2025), 125–139.
- [70] PESSACH, D., AND SHMUELI, E. Algorithmic fairness. In *Machine Learning for Data Science Handbook: Data Mining and Knowledge Discovery Handbook*. Springer, 2023, pp. 867–886.
- [71] PUCCINELLI, D., AND HAENGGI, M. Wireless sensor networks: applications and challenges of ubiquitous sensing. *IEEE Circuits and systems magazine* 5, 3 (2005), 19–31.
- [72] RAJKOMAR, A., HARDT, M., HOWELL, M. D., CORRADO, G., AND CHIN, M. H. Ensuring fairness in machine learning to advance health equity. *Annals of internal medicine* 169, 12 (2018), 866–872.
- [73] RANGAMANI, A., ET AL. *Loss landscapes and generalization in neural networks: Theory and applications*. PhD thesis, Johns Hopkins University, 2020.
- [74] RAUF, H. T., BOGATU, A., PATON, N. W., AND FREITAS, A. Gem: Gaussian mixture model embeddings for numerical feature distributions. *arXiv preprint arXiv:2410.07485* (2024).
- [75] SAGAWA, S., KOH, P. W., HASHIMOTO, T. B., AND LIANG, P. Distributionally robust neural networks for group shifts: On the importance of regularization for worst-case generalization. *arXiv preprint arXiv:1911.08731* (2019).
- [76] SHEKHAR, S., BANSODE, A., AND SALIM, A. A comparative study of hyper-parameter optimization tools. In *2021 IEEE Asia-Pacific Conference on Computer Science and Data Engineering (CSDE)* (2021), IEEE, pp. 1–6.
- [77] SINGH, J. P. Ai ethics and societal perspectives: a comparative study of ethical principle prioritization among diverse demographic clusters. *Journal of Advanced Analytics in Healthcare Management* 5, 1 (2021), 1–18.
- [78] SOHONI, N., DUNNMON, J., ANGUS, G., GU, A., AND RÉ, C. No subclass left behind: Fine-grained robustness in coarse-grained classification problems. *Advances in Neural Information Processing Systems* 33 (2020), 19339–19352.
- [79] STISEN, A., BLUNCK, H., BHATTACHARYA, S., PRENTOW, T. S., KJÆRGAARD, M. B., DEY, A., SONNE, T., AND JENSEN, M. M. Smart devices are different: Assessing and mitigating mobile sensing heterogeneities for activity recognition. In *Proceedings of the 13th ACM conference on embedded networked sensor systems* (2015), pp. 127–140.
- [80] STOPCZYNSKI, A., PIETRI, R., PENTLAND, A., LAZER, D., AND LEHMANN, S. Privacy in sensor-driven human data collection: A guide for practitioners. *arXiv preprint arXiv:1403.5299* (2014).
- [81] SUPEKSALA, Y., NGUYEN, D. C., DING, M., RANBADUGE, T., CHUA, C., ZHANG, J., LI, J., AND POOR, H. V. Private knowledge sharing in distributed learning: A survey. *arXiv preprint arXiv:2402.06682* (2024).
- [82] SURESH, H., AND GUTTAG, J. A framework for understanding sources of harm throughout the machine learning life cycle. In *Proceedings of the 1st ACM Conference on Equity and Access in Algorithms, Mechanisms, and Optimization* (2021), pp. 1–9.
- [83] THOMAS, V., PEDREGOSA, F., MERRIËNBOER, B., MANZAGOL, P.-A., BENGIO, Y., AND ROUX, N. L. On the interplay between noise and curvature and its effect on optimization and generalization. In *Proceedings of the Twenty Third International Conference on Artificial Intelligence and Statistics* (June 2020), PMLR, pp. 3503–3513. ISSN: 2640-3498.
- [84] TRAN, C., FIORETTO, F., KIM, J.-E., AND NAIDU, R. Pruning has a disparate impact on model accuracy. *Advances in Neural Information Processing Systems* 35 (2022), 17652–17664.
- [85] U.S. DEPARTMENT OF HEALTH AND HUMAN SERVICES. Nondiscrimination in health programs and activities. Federal Register, May 2024.
- [86] VENKATASUBBU, S., AND KRISHNAMOORTHY, G. Ethical considerations in ai addressing bias and fairness in machine learning models. *Journal of Knowledge Learning and Science Technology ISSN: 2959-6386 (online)* 1, 1 (2022), 130–138.
- [87] VOS, G., TRINH, K., SARNYAI, Z., AND AZGHADI, M. R. Generalizable machine learning for stress monitoring from wearable devices: A systematic literature review. *International Journal of Medical Informatics* (2023), 105026.

- [88] WANG, H., ZHOU, M., JIA, X., WEI, H., HU, Z., LI, W., CHEN, Q., AND WANG, L. Recent progress on artificial intelligence-enhanced multimodal sensors integrated devices and systems. *Journal of Semiconductors* 46, 1 (2025), 011610.
- [89] XIAN, R., YIN, L., AND ZHAO, H. Fair and optimal classification via post-processing. In *International conference on machine learning* (2023), PMLR, pp. 37977–38012.
- [90] XIAO, Y., SHARMA, H., KAUR, S., BERGEN-CICO, D., AND SALEKIN, A. Human heterogeneity invariant stress sensing. *Proceedings of the ACM on Interactive, Mobile, Wearable and Ubiquitous Technologies* 9, 3 (2025), 1–42.
- [91] XIAO, Y., SHARMA, H., ZHANG, Z., BERGEN-CICO, D., RAHMAN, T., AND SALEKIN, A. Reading between the heat: Co-teaching body thermal signatures for non-intrusive stress detection. *Proceedings of the ACM on Interactive, Mobile, Wearable and Ubiquitous Technologies* 7, 4 (2024), 1–30.
- [92] XU, X., LIU, X., ZHANG, H., WANG, W., NEPAL, S., SEFIDGAR, Y., SEO, W., KUEHN, K. S., HUCKINS, J. F., MORRIS, M. E., ET AL. Globem: Cross-dataset generalization of longitudinal human behavior modeling. *Proceedings of the ACM on Interactive, Mobile, Wearable and Ubiquitous Technologies* 6, 4 (2023), 1–34.
- [93] YFANTIDOU, S., CONSTANTINIDES, M., SPATHIS, D., VAKALI, A., QUERCIA, D., AND KAWSAR, F. Beyond accuracy: A critical review of fairness in machine learning for mobile and wearable computing. *arXiv preprint arXiv:2303.15585* (2023).
- [94] YFANTIDOU, S., CONSTANTINIDES, M., SPATHIS, D., VAKALI, A., QUERCIA, D., AND KAWSAR, F. The state of algorithmic fairness in mobile human-computer interaction. In *Proceedings of the 25th International Conference on Mobile Human-Computer Interaction* (2023), pp. 1–7.
- [95] YFANTIDOU, S., SERMPEZIS, P., VAKALI, A., AND BAEZA-YATES, R. Uncovering bias in personal informatics. *Proceedings of the ACM on Interactive, Mobile, Wearable and Ubiquitous Technologies* 7, 3 (2023), 1–30.
- [96] YU, X., SERRA, T., RAMALINGAM, S., AND ZHE, S. The combinatorial brain surgeon: Pruning weights that cancel one another in neural networks. In *International Conference on Machine Learning* (2022), PMLR, pp. 25668–25683.
- [97] YU, Y., CHEN, B., AND LU, W. On the eigenstructure of the fisher information matrix and its role in generalization error. In *2025 40th Youth Academic Annual Conference of Chinese Association of Automation (YAC)* (2025), IEEE, pp. 3026–3033.
- [98] ZAFAR, M. B., VALERA, I., GÓMEZ-RODRÍGUEZ, M., AND GUMMADI, K. P. Fairness constraints: Mechanisms for fair classification. In *Proceedings of the 20th International Conference on Artificial Intelligence and Statistics (AISTATS)* (2017), pp. 962–970.
- [99] ZAFAR, M. B., VALERA, I., GÓMEZ-RODRÍGUEZ, M., AND GUMMADI, K. P. Fairness constraints: A flexible approach for fair classification. *Journal of Machine Learning Research* 20, 75 (2019), 1–42.
- [100] ZHANG, A., WU, Z., WU, E., WU, M., SNYDER, M. P., ZOU, J., AND WU, J. C. Leveraging physiology and artificial intelligence to deliver advancements in health care. *Physiological Reviews* 103, 4 (2023), 2423–2450.
- [101] ZHANG, J., AND BAREINBOIM, E. Equality of opportunity in classification: A causal approach. *Advances in neural information processing systems* 31 (2018).
- [102] ZHANG, T., XUE, M., ZHANG, J., ZHANG, H., WANG, Y., CHENG, L., SONG, J., AND SONG, M. Generalization matters: Loss minima flattening via parameter hybridization for efficient online knowledge distillation. In *Proceedings of the IEEE/CVF Conference on Computer Vision and Pattern Recognition* (2023), pp. 20176–20185.
- [103] ZHANG, Y., ZHENG, Y., QIAN, K., ZHANG, G., LIU, Y., WU, C., AND YANG, Z. Widar3. 0: Zero-effort cross-domain gesture recognition with wi-fi. *IEEE Transactions on Pattern Analysis and Machine Intelligence* 44, 11 (2021), 8671–8688.

## A Methodological Transparency & Reproducibility Appendix (META)

### A.1 Data and Model Details

This section provides additional details on the datasets, preprocessing pipelines, feature composition, and neural architectures used in **FLARE**. All datasets were standardized to support a consistent autoencoder–classifier formulation and trained under identical preprocessing and optimization protocols, ensuring comparability across sensing domains.

**A.1.1 OhioT1DM Dataset.** The OhioT1DM dataset [61] includes multimodal records from individuals with Type 1 Diabetes collected in 2018 and 2020. The data contain continuous glucose monitoring (CGM) readings, insulin pump records, and contextual annotations (e.g., meals, work, and exercise events). We use 11 participants (4 folds)—with demographic and device information reported in [61]. Preprocessing follows Appendix 2.4 of Arefeen and Ghasemzadeh [10], including temporal alignment of CGM and pump data, removal of incomplete sequences, and normalization within each participant session.

*Feature Representation.* Each instance consists of seven features:

- (1) `basal_insulin` – continuous basal insulin delivery rate;
- (2) `insulin_bolus` – short-acting bolus insulin dosage;
- (3) `time_since_last_bolus` – elapsed time since previous insulin injection;
- (4) `meal_intake` – carbohydrate content of meals (grams);
- (5) `work` – binary contextual indicator of work activity;
- (6) `exercise` – binary contextual indicator of exercise activity;
- (7) `three_hour_glucose` – CGM measurement three hours post-meal.

The binary prediction label indicates normal glucose ( $\leq 180$  mg/dL) or hyperglycemia ( $> 180$  mg/dL).

*Demographic and Device Attributes.* The following attributes were used for subgroup evaluation:

- **Sex:** male, female (six male and six female participants);
- **Age:** 20–40, 40–60, and 60–80 years (participant-level groups);
- **Pump Model:** Medtronic 530G or 630G (two generations of insulin pumps);
- **Sensor Band:** Empatica or Basis (wrist-worn sensor brands);
- **Cohort:** 2018 vs. 2020 (two data-collection cohorts).

These subgroups capture both physiological (sex, age) and technical (pump, sensor) variation, which often drive systematic performance differences in glucose prediction tasks.

*Model Architecture (ExActModel).* ExActModel is a fully connected autoencoder–classifier network. The encoder has four layers (256–128–64–32) with Tanh activations and dropout rates of 0.5, 0.3, and 0.3, respectively. The decoder mirrors this structure, and the classifier is a two-layer MLP (32–8–2) with ReLU and dropout (0.3). Training minimizes a weighted combination of reconstruction loss (MSE) and cross-entropy loss.

*A.1.2 Intern Health Study (IHS) Dataset.* The Intern Health Study (IHS) [1] is a 14-month longitudinal dataset tracking medical interns from two months before internship through the end of their first year. It includes demographics, PHQ-9 mental health assessments, and daily mood self-reports (1–10). Fitbit data provide daily summaries of sleep, step count, and heart rate. We analyze cohorts from 2018–2022.

*Data Preprocessing.* We use 85 participants (17 per fold). Daily mood labels are binarized following Manjunath et al. [60]: moods  $> 8$  are labeled positive (1), moods  $< 3$  negative (0), and intermediate values excluded. Sensor data are aggregated to daily averages; missing values are imputed with mean substitution, and binary “missing-indicator” flags are added. All numeric features are z-normalized per participant.

*Feature Representation.* Eighteen input features are used: 9 Fitbit-derived measures (e.g., sleep duration, sleep phases, resting heart rate, step count) and 9 corresponding missing-indicator variables. These features capture daily physical activity and rest patterns linked to stress and mood variation.

*Demographic and Behavioral Attributes.* Subgroups for model evaluation include:

- **Sex:** male, female (self-identified at baseline);
- **Age:** 24–29, 30–34, and 35+ years (age at baseline);
- **Ethnicity:** Caucasian, African American, Latino/Hispanic, Asian, Mixed/Other;
- **Residency Specialty:** Internal Medicine, Surgery, Obstetrics/Gynecology (Ob/Gyn), Pediatrics, Psychiatry, Neurology, Emergency Medicine, Medicine/Pediatrics (Med/Peds), Family Practice, Transitional, Anesthesiology, Otolaryngology;
- **Baseline Depression (PHQ10>0):** yes, no (presence of depressive symptoms prior to internship).

These attributes represent both demographic diversity and occupational heterogeneity, capturing psychosocial and contextual factors associated with stress, sleep, and mood variation among medical interns.

*Model Architecture (IHS\_MLP)*. The IHS\_MLP encoder uses three layers (128–64–32) with ReLU activations and dropout (0.1); the decoder mirrors this structure. The classifier has three layers (32–16–8–2) with ReLU and dropout (0.1). Models are optimized using Adam ( $\eta = 10^{-3}$ ), and hyperparameters are tuned via *Optuna* [76] to maximize F1 performance.

*A.1.3 EDA Dataset*. The EDA dataset [90, 91] captures multimodal physiological signals, including electrodermal activity (EDA), heart rate (HR), temperature (TEMP), acceleration (ACC), and heart rate variability (HRV). Data were collected from 76 participants under both control and intervention conditions, producing 340 handcrafted features for binary stress classification.

*Feature Composition*. Features cover tonic and phasic components of EDA and higher-order statistics such as mean, variance, skewness, kurtosis, peak count, energy, and entropy (permutation and SVD entropy). Similar features are extracted for HR, TEMP, ACC, and HRV modalities. All features are z-normalized per participant.

*Demographic and Experimental Attributes*. Evaluation subgroups are defined as:

- **Group**: control, pre-dose, and post-dose (experimental conditions);
- **Sex**: male, female.

These categories quantify fairness across both experimental interventions and intrinsic biological variation.

*Model Architecture (EDA\_MLP)*. The encoder maps the 340-dimensional input into a 128-dimensional latent space using three fully connected layers with ReLU activations and dropout (0.1). The decoder reconstructs the input, and the classifier (128–64–64–2) outputs stress vs. non-stress logits. Training minimizes a combined reconstruction and cross-entropy loss with Fisher penalty-based stability regularization.

For all three datasets, we include **User Heterogeneity (UH)**: per-participant slices capturing subject-level disparities in physiological response and signal quality.

## A.2 Training Protocol and Implementation Details

All models were trained with the Adam optimizer and early stopping based on validation F1. The total loss combined reconstruction, cross-entropy, and Fisher penalty terms, with dataset-specific weighting. Fisher information was computed only on correctly classified samples, as described in Algorithm 1.

Table 5. Summary of datasets and base model configurations.

Dataset	Participants	Features	Task	Model (Encoder–Classifier)
OhioT1DM [61]	11	7	Glucose (binary)	input–256–128–64–32 / 32–8–2
IHS [1]	85	18	Mood (binary)	input–128–64–32 / 32–16–8–2
EDA [90, 91]	76	340	Stress (binary)	input–128 / 128–64–64–2

Random seeds were fixed for reproducibility, and all results were averaged across folds. This unified framework ensures that cross-dataset differences observed under **FLARE** reflect true sensing heterogeneity rather than architectural variation.

## A.3 Subgroup-Level Performance Analysis

Tables 6 and 7 summarize the subgroup-level F1 scores for the Baseline, KD, ARL, Reckoner, GoG, and **FLARE** models across the OhioT1DM, EDA, and IHS datasets. Each table reports performance disaggregated by demographic attributes (e.g., sex, age, ethnicity, specialty), allowing evaluation of both model utility and consistency across heterogeneous populations.

Across all datasets, **FLARE** consistently attains the highest or among the highest F1 scores within each subgroup, indicating improved predictive stability relative to all baselines. In the OhioT1DM dataset, **FLARE** yields notable gains across age and device-related groups, demonstrating robustness to variation in sensor type and user cohort. In the EDA dataset, where the baseline performance is already strong, **FLARE** maintains stable accuracy across experimental conditions (Control, Predose, Postdose) and between sexes, outperforming adversarial and distillation-based approaches that exhibit inconsistent subgroup behavior. Finally, in the more heterogeneous IHS dataset, **FLARE** achieves superior F1 scores across sex, age, ethnicity, and specialty subgroups, reflecting its capacity to generalize across diverse populations.

These results highlight that **FLARE** not only improves overall utility but also reduces variability across subgroups compared with fairness-oriented baselines such as ARL and GoG.

Table 6. F1 scores across subgroups for different models (Baseline, KD, ARL, Reckoner, GOG, **FLARE**) in the OhioT1DM and EDA datasets.

Dataset	Group	Baseline F1	KD F1	ARL F1	Reckoner F1	GOG F1	FLARE F1
<b>OhioT1DM Dataset</b>							
Sex	Female	0.6839	0.6985	0.7085	0.7136	0.6882	0.7127
	Male	0.6119	0.6631	0.7057	0.6937	0.6137	0.7417
Age	20–40	0.3942	0.5089	0.5896	0.6922	0.3983	0.7407
	40–60	0.6723	0.6976	0.7121	0.6931	0.6776	0.7263
	60–80	0.7103	0.7437	0.8030	0.7815	0.6976	0.7638
Pump	530G	0.6777	0.7043	0.7263	0.7069	0.6800	0.7318
	630G	0.3942	0.5089	0.5896	0.6922	0.3983	0.7407
Sensory Band	Basis	0.7073	0.7212	0.7305	0.7126	0.7133	0.7337
	Empatica	0.5589	0.6253	0.6786	0.6884	0.5567	0.7244
<b>EDA Dataset</b>							
Group_label	Control	0.8822	0.7436	0.8779	0.9706	0.8627	0.8899
	Predose	0.8367	0.7425	0.8420	0.4952	0.8315	0.8550
	Postdose	0.9194	0.7996	0.9271	0.8645	0.9217	0.9264
Sex	Female	0.8789	0.7496	0.8741	0.7439	0.8626	0.8857
	Male	0.8973	0.7743	0.9025	0.6651	0.8894	0.9057

#### A.4 Training Efficiency and Runtime Analysis of **FLARE**

To complement our inference analysis, we further benchmarked the training-time performance of **FLARE** against baseline models. Table 8 summarizes the average training latency, memory footprint (RSS), and resource utilization across multiple hardware platforms. As shown, the base pretraining phase of **FLARE** (BpT) introduces a higher runtime overhead—e.g., 799.97 s on the RTX 4090 and 847.83 s on the Ryzen 9—due to latent subgroup identification and Fisher-guided clustering. However, the CPU utilization (0.8–3.0%) and memory usage (~1400 Mb) remain on par with other baselines such as ARL and KD, indicating that the additional computation arises from algorithmic complexity rather than hardware inefficiency. This overhead is acceptable in practice, as human-sensing systems typically perform model training or personalization on centralized servers or cloud-based infrastructures before on-device deployment [7, 47, 63, 66]. Consequently, **FLARE** maintains energy and resource efficiency during training while providing improved robustness and fairness benefits in deployment.

Table 7. F1 scores across subgroups for different models (Baseline, KD, ARL, Reckoner, GOG, **FLARE**) in the IHS dataset.

<b>Subgroup</b>	<b>Group</b>	<b>Baseline F1</b>	<b>KD F1</b>	<b>ARL F1</b>	<b>Reckoner F1</b>	<b>GOG F1</b>	<b>FLARE F1</b>
Sex	Male	0.5975	0.5694	0.6203	0.5764	0.5857	0.6247
	Female	0.5957	0.5910	0.6324	0.5673	0.6128	0.6418
Age	23	0.8151	0.5884	0.8182	0.7273	0.4969	0.9091
	24	0.3194	0.2941	0.4158	0.3678	0.3529	0.4436
	25	0.5872	0.5772	0.5901	0.6101	0.5756	0.6033
	26	0.6515	0.6071	0.6588	0.5803	0.6635	0.6915
	27	0.6517	0.6339	0.6651	0.6024	0.6095	0.6716
	28	0.5617	0.5374	0.6156	0.5382	0.6139	0.5910
	29	0.5195	0.5490	0.5887	0.5305	0.5685	0.5856
	30	0.5635	0.5846	0.6239	0.5386	0.5575	0.6177
	32	0.6057	0.5785	0.6513	0.6136	0.5909	0.6627
	33	0.5086	0.5441	0.5441	0.4256	0.3285	0.5810
	34	0.3565	0.3565	0.4706	0.3934	0.5569	0.5505
	38	0.7980	0.8356	0.8380	0.6576	0.7340	0.8044
	51	0.4793	0.4793	0.5084	0.5084	0.4793	0.4793
Ethnicity	White	0.6099	0.5889	0.6407	0.5860	0.6062	0.6435
	Black / African American	0.5085	0.5548	0.5788	0.4957	0.4778	0.5085
	Latino / Hispanic	0.6283	0.5364	0.7110	0.5892	0.7692	0.7110
	Asian	0.5823	0.5730	0.6007	0.5587	0.5868	0.6205
	Multi-racial	0.5768	0.5773	0.6197	0.5347	0.6189	0.6543
	Arab / Middle Eastern	0.2262	0.4762	0.4954	0.3174	0.4012	0.3174
Specialty	Internal Medicine	0.5893	0.5617	0.6175	0.5730	0.5840	0.6379
	Surgery	0.6014	0.6113	0.6161	0.5667	0.6238	0.6247
	Ob/Gyn	0.6078	0.5549	0.6834	0.5368	0.7281	0.6834
	Pediatrics	0.6324	0.6101	0.6666	0.5869	0.6320	0.6767
	Psychiatry	0.6377	0.5770	0.6377	0.5608	0.6377	0.6445
	Neurology	0.5685	0.6522	0.6072	0.5934	0.6033	0.6522
	Emergency Medicine	0.5042	0.5816	0.6263	0.5976	0.5723	0.5967
	Med/Peds	0.5723	0.6213	0.6955	0.5404	0.6234	0.6963
	Family Practice	0.4791	0.4955	0.5825	0.4999	0.5607	0.5828
	Other	0.6199	0.6272	0.6353	0.6215	0.5904	0.6522
	Transitional	0.6191	0.6469	0.6722	0.5892	0.6148	0.6890
	Anesthesiology	0.4504	0.5424	0.5467	0.5586	0.4966	0.5358
PHQ10>0	Yes	0.6588	0.6098	0.6645	0.6167	0.5854	0.6880
	No	0.5916	0.5787	0.6239	0.5677	0.6017	0.6295

Table 8. Train Time (s), Train Process (RSS) Memory Usage (MB), and Train Resource Usage (%) for baselines and **FLARE** during Base pretraining (BpT) and Adaption (Adapt) phases across different platforms.

Platform	ARL			KD			Reckoner			GoG			FLARE (BpT)			FLARE (Adapt)		
	Train (s)	RSS (MB)	Usage (%)	Train (s)	RSS (MB)	Usage (%)	Train (s)	RSS (MB)	Usage (%)	Train (s)	RSS (MB)	Usage (%)	Train (s)	RSS (MB)	Usage (%)	Train (s)	RSS (MB)	Usage (%)
<b>EDA Dataset</b>																		
NVIDIA GeForce RTX 4090	7.348	1256	5.23	11.86	1264	25	170	1286.2	12.3	22.58	1618.5	16	799.97	1412	16.20	0.12	1035	4
AMD Ryzen 9 7950X 16-Core Processor	10.446	1263.2	0.78	14.95	1274.7	1.72	159.32	1351.7	0.79	16.96	1648	0.78	847.83	1428.4	0.86	0.5	1073	0.66
Quadro RTX 5000	21.65	1020.3	12	71.06	1030.4	29.30	721.78	1146.4	2.50	72.7	1431.9	8.50	694.84	1285.3	4.0	0.54	818.8	1.80
Intel i9-9900K Processor	106.7	1111.2	3.11	157.8	1143.6	3.12	2205.04	1234.7	3.04	151.8	1712.8	3.75	1481.6	1341.8	3.12	0.1	840.1	2.96
Apple M1	26.01	157.7	1.41	45.13	142.5	1.27	354.278	72.6	1.99	46.92	95.4	2.16	461.17	67.1	5.80	0.1320	331.5	0.42